Cronfa - Swansea University Open Access Repository

_____

This is an author produced version of a paper published in :
IEEE Journal of Translational Engineering in Health and Medicine

Cronfa URL for this paper:

_____

Paper:

_____

Computer Vision Techniques for Transcatheter Intervention

Feng Zhao, Xianghua Xie, *Senior Member, IEEE,* and Matthew Roach

Abstract—Minimally invasive transcatheter technologies have demonstrated substantial promise for the diagnosis and treatment of cardiovascular diseases. For example, TAVI is an alternative to AVR for the treatment of severe aortic stenosis and TAFA is widely used for the treatment and cure of atrial fibrillation. In addition, catheter-based IVUS and OCT imaging of coronary arteries provides important information about the coronary lumen, wall and plaque characteristics. Qualitative and quantitative analysis of these cross-sectional image data will be beneficial for the evaluation and treatment of coronary artery diseases such as atherosclerosis. In all the phases (preoperative, intraoperative, and postoperative) during the transcatheter intervention procedure, computer vision techniques (e.g., image segmentation, motion tracking) have been largely applied in the field to accomplish tasks like annulus measurement, valve selection, catheter placement control, and vessel centerline extraction. This provides beneficial guidance for the clinicians in surgical planning, disease diagnosis, and treatment assessment. In this paper, we present a systematical review on these state-of-the-art methods.

We aim to give a comprehensive overview for researchers in the area of computer vision on the subject of transcatheter intervention. Research in medical computing is multi-disciplinary due to its nature, and hence it is important to understand the application domain, clinical background, and imaging modality so that methods and quantitative measurements derived from analyzing the imaging data are appropriate and meaningful. We thus provide an overview on background information of transcatheter intervention procedures, as well as a review of the computer vision techniques and methodologies applied in this area.

Index Terms—Image processing, IVUS, medical imaging, OCT, reconstruction, registration, segmentation, transcatheter intervention, TAFA, TAVI, TMVR, TPVR, TTVI.

I. INTRODUCTION

TRANSCATHETER intervention is an emerging technology for the diagnosis and treatment of cardiovascular diseases. In recent years, more and more computer vision techniques have been used in all the phases of the transcatheter intervention procedures. It is thus desirable to give an overview of this increasingly important research area. The purpose of this paper is to present a comprehensive background of this clinical application, including pathology and imaging modality, and a detailed survey of the computer vision techniques popularly applied in such procedures. Particularly for new comers to this area with a computer vision background, it is beneficial to gain understanding of the basics of transcatheter intervention technologies, as well as to have a thorough

F. Zhao, X. Xie (corresponding author, x.xie@swansea.ac.uk), and M. Roach are with the Department of Computer Science, Swansea University, Swansea, SA2 8PP, United Kingdom.
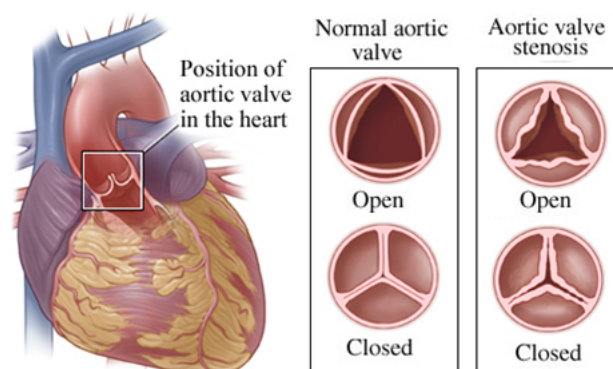

Fig. 1. Normal and diseased aortic valves (images are adapted from WebMD [4]).

understanding of the crucial role that various computer vision methods played in transcatheter interventions.

Cardiovascular disease generally refers to abnormalities in the heart and blood vessels, mainly including coronary heart disease, stroke, peripheral arterial disease, and aortic disease. It is one of the leading causes of death in developed countries, killing more than 88,000 and 600,000 people in the UK and USA each year, respectively [1], [2]. Aortic stenosis is the most common valvular heart disease [3], where the aortic valve cannot fully open, usually a result of calcium deposit (calcification) in the artery that makes the valve narrow (see Fig. 1). The blood flow from the heart hence decreases, leading to severe hypertension and angina. If untreated, it could cause functional deterioration, heart failure, and even death.

Transcatheter intervention is an emerging technology that can provide promising solutions for cardiovascular diseases. In all the phases (preoperative, intraoperative, and postoperative) during this procedure, computer vision techniques such as image segmentation and motion tracking have been widely applied to accomplish many tasks including annulus measurement, valve selection, catheter placement control, and vessel centerline extraction, which provides beneficial guidance for the clinicians in surgical planning, disease diagnosis, and treatment assessment. In this review, we focus on the importance and benefits of computer vision techniques popularly used in transcatheter intervention in clinical practice. However, it is also necessary to introduce background information of transcatheter intervention procedures, e.g., imaging modalities, principles of imaging, advantages and disadvantages, properties of acquired images, and challenges of processing these image data.

Transcatheter intervention is generally performed through the lumen of a catheter, including the delivery of intravascular
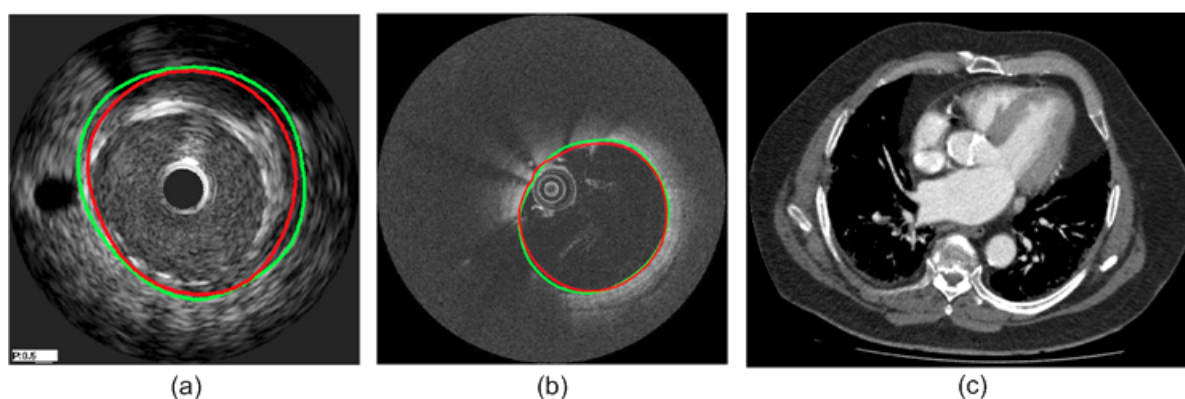
Fig. 2. Typical cross-sectional images delivered by different imaging technologies. (a) IVUS image of coronary artery [6], (b) OCT image of coronary artery [6], and (c) X-ray CT image of aortic root (image is from Morriston Hospital [7]).

devices such as balloon, coils and stents to dilate or close cardiovascular defects. The catheter-based imaging technologies such as intravascular ultrasound (IVUS) and optical coherence tomography (OCT) [5] can provide 2D cross-sectional images of the coronary artery structure. As a valuable complementary modality to angiography, both modalities measure the back-scattered signal from the surrounding vessel structure after sending a sound wave in IVUS or light in OCT. They have been widely used in coronary disease diagnosis and treatment, since the clinicians can apply them to assess the severity of a lesion, perform plaque classification, and determine the location and size for stenting. The acquired IVUS and OCT images contain precise information including the lumen size, stent strut location, and morphology analysis of plaque lesion. However, the IVUS images are noisy with attenuation, speckles and other artifacts. OCT images have a relatively higher resolution than IVUS images, but they still suffer from guide-wire and shadowing artifacts that may cause missing or weakening the boundaries. Therefore, it is critical to extract the boundaries, although the accurate segmentation of the inner/outer arterial wall is still a challenge problem.

As shown in Fig. 2a, a typical IVUS image consists of three parts: lumen, vessel that includes intima and media layers, and adventitia that surrounds the vessel wall. The media-adventitia border represents the outer coronary arterial wall located between the media and adventitia. Segmentation of IVUS images has shown to be an intricate process due to the low contrast and various forms of interferences and artifacts caused by different factors such as calcification and acoustic shadow. Catheter movement can also cause spatial and temporal fluctuation, leading to ambiguities. To tackle the problems, various algorithms have been developed in the literature [8]. Among many others, graph cut-based technique has shown to be a promising approach to IVUS image segmentation, where the inner/outer vessel wall is extracted with careful manual initialization [9] or automatically detected without requiring user initialization [10]–[12]. Both of them are based on the minimization of a cost function derived from different feature information (e.g., edge/boundary, shape prior, texture).

OCT provides high-resolution cross-sectional imaging of vessels including the coronary arteries and it can accurately differentiates the most superficial layers of the vessel wall as well as stent struts and the vascular tissue surrounding them (see Fig. 2b). For the management of cardiovascular disease, it is important to obtain the vessel wall properties. Approaches based on mathematical morphology, thresholding, Catmull-Rom splines, and active contour models are commonly used for the detection of the vessel wall and stent strut in OCT images with no existence of guide-wire shadow artifacts [13]–[15]. In fact, OCT image sequences may have guide-wire shadow artifacts which result in inaccurate vessel wall segmentation. To overcome the difficulty, Tung et al. [16] proposed an automatic method utilizing active contour models, convex hull detection along with expectation maximization and graph cut for the elimination of guide-wire shadow artifacts and the accurate detection of the vessel wall as well as stent strut, in which the removal of shadow artifacts relies on the good estimation of the guide-wire position.

Traditionally, surgical aortic valve replacement (AVR) is the only effective treatment for adults with severe symptomatic aortic stenosis that carries a poor prognosis. For patients (up to 30% [17]) who are not eligible for such an open-heart surgery to replace their aortic valve, transcatheter aortic valve implantation/replacement (TAVI/TAVR[1]) is an alternative to AVR and will represent the new standard for the treatment of severe aortic stenosis. To reduce the risk of stroke and major vascular complications after TAVI (e.g., severe aortic regurgitation, atrioventricular block), it is very important to select the optimal access route for valve implantation and place the valve in the right position. This depends on the accurate extraction of the vessel geometry of the thoracic aorta and heart (especially the aortic root). Computer vision techniques including advanced image processing, real-time interactive segmentation [18], and motion tracking provide an opportunity to approach this goal for both the preoperative planning and intraoperative treatment. Fig. 2c gives an example slice image for the TAVI procedure through X-ray computed tomography (CT) imaging modality.

The remainder of this survey is organized as follows. In Section II, we briefly introduce the transcatheter intervention technologies including heart valve implantation/replacement, atrial fibrillation ablation, IVUS and OCT. The variety of

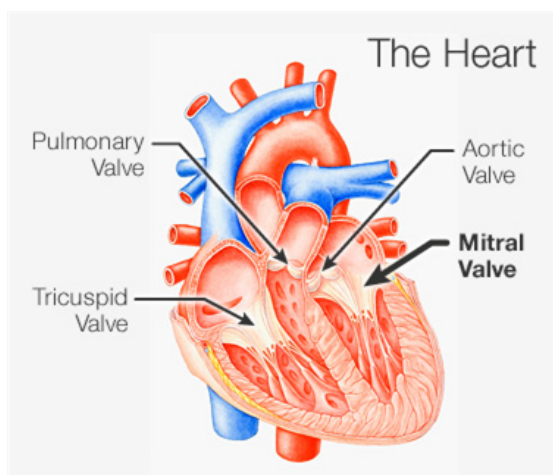[1]We use TAVI for the rest of this paper.

Fig. 3. The four valves in a human heart (image is adapted from Web-MD [19]).

computer vision techniques in transcatheter intervention is given in Section III. In Section IV, we discuss different imaging modalities involved in the transcatheter procedure as well as performance evaluation of segmentation methods. We finally conclude this paper in Section V.

II. TRANSCATHETER INTERVENTION TECHNOLOGIES

The four heart valves (see Fig. 3) determine the pathway of blood flow through the heart. Normally, a heart valve allows blood flow in only one direction. Heart disease occurs when a valve cannot fully open due to calcification in the artery and thus decreases the blood flow (called stenosis) or a valve malfunctions and allows some blood to flow in the wrong direction (called regurgitation). Compared to traditional surgical operations for the treatment of heart diseases, transcatheter technologies offer a minimally invasive way for replacing abnormal heart valves, leading to less morbidity and faster recovery. In the following sections, we give a brief introduction of these transcather approaches currently employed or potentially adopted in clinical practice.

A. Transcatheter aortic valve implantation

Aortic valve stenosis (see Fig. 1) is the most commonly acquired heart valve disease. The gold standard for the treatment of severe symptomatic aortic stenosis is the implantation of an aortic valve prosthesis via open-heart surgery, i.e., surgical aortic valve replacement (AVR). However, a large number of patients (approximately one-third) are not eligible for surgical AVR because of their advanced age or other diseases like renal dysfunction. In such cases, transcatheter aortic valve implantation (TAVI) [20], [21] is a cost-effective alternative to AVR and plays an important role in the treatment of aortic stenosis by increasing life expectancy and improving quality of life. It has been proven to be feasible, safe and effective for the treatment of patients with JTH severe aortic stenosis [17], [22]–[24]. TAVI has evolved as a routine procedure for high risk patients [22], [25] and it outperforms medical therapy in these patients with respect to mortality [26].

TAVI is the implantation of an aortic heart valve prosthesis within the diseased aortic valve through a catheter without the need of open-heart surgery. There are two main approaches for implanting a valve in the aortic root: transfemoral and transapical approaches. The former technique is a retrograde approach via the femoral artery, the subclavian artery, or the ascending aorta; and the latter one is an antegrade approach via the apex of the heart. As a minimally invasive approach, TAVI surgery is performed using echocardiographic and fluoroscopic guidance for visualization during implantation. During the procedure, a valve (a balloon expandable stent combined with a bovine pericardial bioprosthetic tissue valve) is reduced to size and placed on a delivery catheter. The delivery catheter is then inserted either in the femoral artery through a small incision at the top of the leg (transfemoral approach) or between the ribs through the apex of the heart (transapical approach). Once in the heart, the valve is positioned and deployed across the patient's diseased aortic valve. Fig. 4 gives an example of such a TAVI procedure through femoral artery. It is very important to place the valve in a right position to reduce the risk of stroke and major vascular complications. For example, a low valve implantation may lead to severe aortic regurgitation (AR), or promote atrioventricular block (AVB) after TAVI [28], [29].

1) Role of imaging: During the whole TAVI procedure, a variety of different imaging modalities [30], [31] are involved, including preoperative imaging, intraoperative imaging, and postoperative imaging. This multi-modality imaging may help to minimize the major complications (e.g., vascular complications, paravalvular leaks, stroke, atrioventricular block) and plays an important role in the TAVI workflow. As shown in Table I, preoperative imaging techniques such as multislice computed tomography (CT), X-ray angiography/fluoroscopy, and transesophageal echo (TEE) are applied for patient selection, artery assessment, access site selection, valve selection, approach selection, and the planning of implant placement, while intraoperative imaging techniques (e.g., X-ray angiography and TEE) are utilized for guiding the catheter placement, controlling the valve positioning, and quality control. These imaging modalities can be used for postoperative follow-up as well.

Precise and extensive preoperative planning is of great importance for the TAVI procedure, starting from careful patient selection. At present, TAVI is suitable for high-risk patients with severe symptomatic aortic stenosis, but is not recommended for patients with bicuspid valves [36], [37]. Transthoracic echocardiography (TTE), transesophageal echocardiography (TEE), magnetic resonance imaging (MRI), or computed tomography (CT) can be applied for diagnosis of aortic stenosis. Once a patient is identified, the next step is to choose the approach type (transfemoral or transapical) according to the criteria and parameters reported in [36]. The feasibility of the transfemoral or transapical approach can be best assessed by multislice CT angiography (CTA). To prevent severe complications after TAVI such as left ventricular outflow tract (LVOT) rupture and postoperative aortic insufficiency (AI) due to paravalvular leaks, it is crucial to decide the proper valve size and type based on the aortic
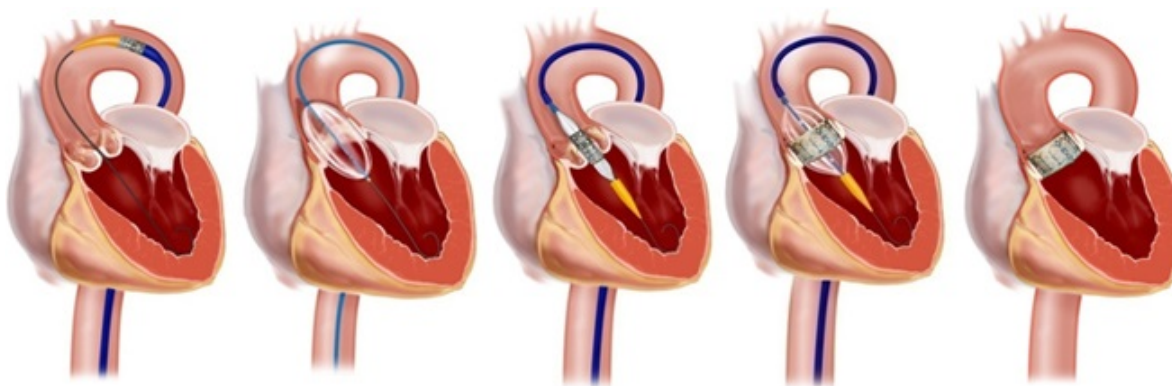
Fig. 4. The TAVI procedure through femoral artery (images are adapted from Raney Zusman [27]).

TABLE I
IMAGING MODALITIES AND THEIR APPLICABILITY FOR THE TAVI PROCEDURE.

Phase	Imaging Modality	Applicability
Preoperative	Computed tomography X-ray angiography Transesophageal echo	Patient selection, artery assessment, access site selection, valve selection, approach selection, implant placement planning
Intraoperative	X-ray angiography Transesophageal echo	Catheter placement guidance, valve position control, quality control
Postoperative	Transesophageal echo Computed tomography	Paravalvular leaks evaluation, valve migration assessment

TABLE II
COMPARISON OF FOUR COMMERCIAL PROSTHETIC HEART VALVING MODELS.

Model	Manufacturer	Transfemoral Approach	Transapical Approach	Clinical Approval
Sapien®	Edwards Lifesciences [32]	Yes	Yes	Europe, USA
CoreValve®	Medtronic [33]	Yes	No	Europe, USA
Jenavalve®	Jenavalve Technology [34]	No	Yes	Europe
Acurate®	Symetis [35]	Yes	Yes	Europe

root geometry and the aortic annulus diameter measured with CTA imaging [38].

To select the optimal intraoperative treatment, angiography is generally used to guide the catheter placement for both transfemoral and transapical aortic valve implantation, while TEE is applied to ensure correct wire placement within the left ventricle (LV). During valve placement, these online imaging techniques also guarantee clear identification of the coronary ostia and the annulus to avoid occlusion of the coronary ostia and impairment of the mitral valve. Therefore, the stented valve can be positioned in the aortic annulus accurately, which is essential for TAVI [31].

After valve deployment, TEE is used to regularly monitor paravalvular leaks as well as valve migration during follow-up. In case of inconclusive findings or indication of major complications, CT imaging can be supportive. The immediate, midterm and long-term TAVI procedural results can then be evaluated appropriately.

Accurate patient selection, good knowledge of the vascular anatomy, aortic annulus size, and LV evaluation will benefit the prosthetic valve selection and procedural approach selection, thus minimize the risk of major complications with TAVI. Moreover, a number of new techniques are being developed, including 3D imaging technology (e.g., the Syngo DynaCT system) [39], template-based planning [40], patient-specific simulation approaches [41], and image-guided catheter interventions [42]. In the future, these techniques could be employed for determining the optimal treatment preoperatively, for more accurate patient selection, intervention planning and valve placement, or for postoperative prediction of the long-term outcome, valve degeneration and migration.

2) State-of-the-art valving techniques: To date, there are four types of commercial transcatheter aortic valve prostheses (TAVP) available in the European market: the Sapien® valve by Edwards Lifesciences (Irvine, California, USA) [32], the CoreValve® revalving system by Medtronic (Minneapolis, Minnesota, USA) [33], the Jenavalve® by Jenavalve Technology (Munich, Germany) [34], and the Acurate TA® by Symetis (Ecublens, Switzerland) [35]. The Sapien® (stainless steel stent) and Sapien XT® (Cobalt-chromium stent) models were approved for both transapical and transfemoral approaches, and Sapien® is the only balloon-expandable TAVP in clinical use. The CoreValve® (Nitinol stent) system is a self-expandable TAVP, which was approved for transfemoral, subclavian and direct aortic approaches. Both Jenavalve® and Acurate TA® are self-expandable TAVP and they were
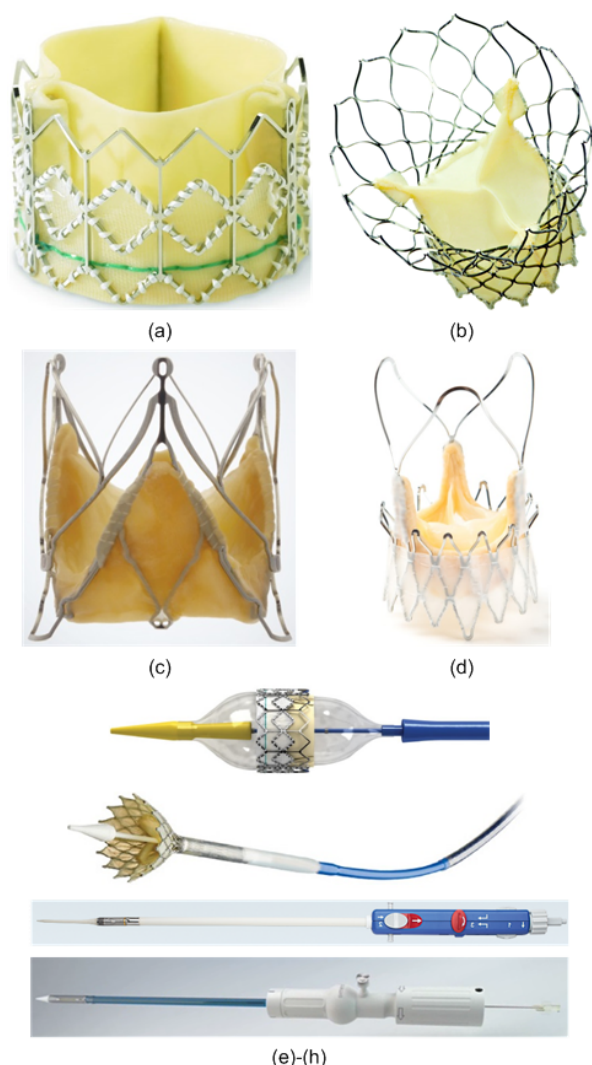
Fig. 5. Examples of different prosthetic heart valves. (a) Sapien® valve, (b) CoreValve®, (c) Jenavalve®, (d) Acurate TA®, and (e)-(h) valves expanded on balloon and catheter or crimped on catheters. (Images are from Edwards Lifesciences [32], Medtronic [33], Jenavalve [34], and Symetis [35], respectively.)

approved for transapical procedure only. Recently, Symetis demonstrated the Acurate TF® at EuroPCR 2013 that can be delivered via transfemoral procedure. Fig. 5 shows examples of these heart valve models and Table II gives a summary of them. The impact of these heart valve prostheses is impressive. More than 40,000 TAVPs have been implanted worldwide, among which Germany is the leading country. In 2010, approximately 25% of all aortic valve replacements were performed with TAVP [43]. The total number of patients currently eligible for TAVI procedure is approximately 200,000, representing a $2B market worldwide.

3) Challenges: The common procedure of TAVI is to place a cylindrical stent device inside the aortic root, i.e., a cylinder inside a cylinder. Without calcifications, the stent device is prone to migrate and dislodge, as the anchoring mechanism is based on friction. The success rate is still low, due to the intrinsic complexity of the procedure, the suboptimal positioning of the prosthesis, and the device migration. In

addition, the risk of malpositioning is still high. These issues can be addressed by a couple of means, e.g., a sophisticated shape of the stent, innovative materials for both the stent and the functional component, an easier and more reliable procedure, etc. From the technological point of view, the significant improvement of imaging quality and the rapid development in computer vision especially the real-time interactive segmentation techniques [18] could lead to a higher rate of procedural success by providing more accurate valve size assessment, self-guided positioning, unique matching with the anatomy of the aortic root, and so on.

Compared to the surgical AVR where the original valve and surrounding calcifications are removed before implanting the valve prosthesis, TAVI overlaps the prosthetic valve to the existing irregular calcifications. Thus, its effective functioning and consequent durability in human use need to be addressed in the future development of the technology.

B. Transcatheter mitral valve repair

Mitral regurgitation (MR) may lead to progressive left ventricular dysfunction, heart failure, and even death. The traditional surgical mitral valve repair or replacement is the established treatment for degenerative MR, whereas it may not be applicable for functional MR and those high-risk patients with both degenerative and functional MR (see Fig. 6), especially elderly persons. Transcatheter mitral valve repair/replacement (TMVR) technology has been developed for such cases. A variety of technologies have emerged and are at different stages of investigation. In [45], Karimov, Massiello, and Fukamachi reviewed various transcatheter-based technologies for mitral valve replacement. Chiam and Ruiz [46] classified the percutaneous TMVR approaches based on functional anatomy. They grouped the therapies into those targeting the leaflets, annuloplasty, percutaneous chords, and LV remodeling. Currently, the MitraClip therapy [47] (see Fig. 7) is the only percutaneous transcatheter treatment for selected patients with degenerative or functional MR [48], [49], which is based on edge-to-edge surgical technique pioneered by Alfieri et al. [50]. Maisano et al. [51] reported the early and 1-year results of the percutaneous mitral valve interventions in 567 patients with significant MR who underwent the MitraClip therapy at 14 European sites. The patients' mean age was 74 years and most of them had functional MR (77%) with multiple comorbidities including coronary artery disease, hypertension, atrial fibrillation, and renal disease. The 30-day mortality rate was 3.4% and no MitraClip device embolization was observed. At 12 months after the procedure, the majority of patients demonstrated improvement in the severity of MR. This study involved the largest database of MitraClip therapy till now and confirmed the safety, efficacy, and low mortality rate of the MitraClip implant procedure in high-risk patient population.

So far, more than 10,000 patients have been treated with TMVR throughout the world [49]. Compared to the progress in TAVI technology, the transcatheter treatment of MR patients is underserved. However, it appears that TMVR will progress into daily clinical practice in the near future. Start-up companies like Endovalve [53] and CardiAQ [54] are in the process
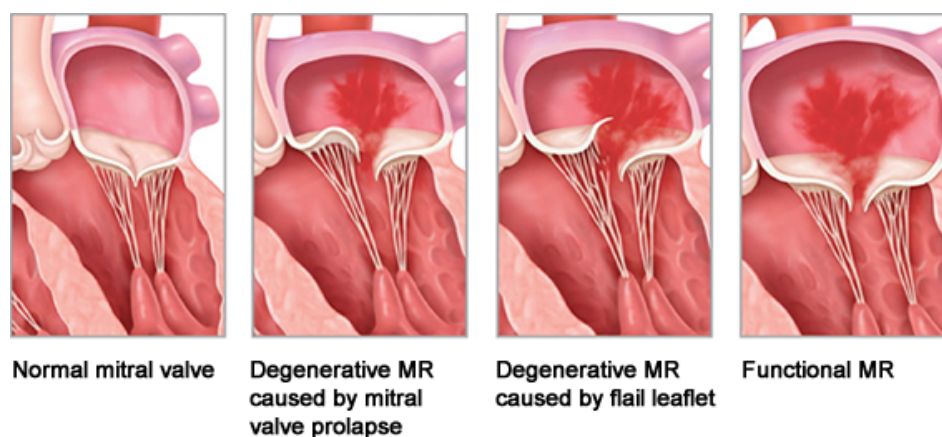
Fig. 6. The normal and degenerative mitral valves (images are adapted from Abbott Vascular [44]).

of developing TMVR products for the treatment of functional MR. Worldwide cardiovascular leading companies (e.g., Edwards Lifesciences [32], Medtronic [33]) are involved in this area as well. Furthermore, advancements in computer vision will offer innovative solutions to properly address prosthesis anchoring and sealing in mitral position for transcatheter mitral valve technologies.

C. Transcatheter pulmonary valve replacement

Transcatheter pulmonary valve replacement (TPVR) is a feasible alternative to surgical bioprosthetic valve implantation (see Fig. 8). There has been a recent explosion in this emerging field. In [55], Ghawi et al. reviewed the progress and innovations of TPVR, its benefits and challenges, as well as the future advancements associated with this technology. The first human transcatheter valve implantation in the pulmonary position was performed via the transfemoral approach for a 12-year-old male patient with pulmonary atresia and ventricular septal defect [56]. More TPVR procedures were reported by the same group [57], where all the eight patients had significant improvement in their pulmonary insufficiency after successful implantation of the valve in the desired position. Following these successful clinical attempts of TPVR, more clinical trials [58]–[62] focused on the effectiveness, safety and

Fig. 7. The MitraClip procedure (images are from Cath Lab Digest [52]).

longevity of the valves (e.g., Medtronic Melody® valve [33], Edwards Sapien® valve [32]).

Although many successes have been noted, there are still a number of challenges with this procedure, including potential procedural complications such as valve migration, guide wire injury to a distal branch pulmonary artery, damage to the tricuspid valve, and arrhythmia [58], [60], along with device-related complications like Hammock effect and stent fracture [61], [64]–[66]. Recent studies demonstrated that the procedural complications can be reduced to 5-6% [67] and the device-related complications can be treated by valve-in-valve TPVR [68].

D. Transcatheter tricuspid valve implantation

Tricuspid regurgitation (TR) is the most common pathology of tricuspid valve, due to the increased right ventricular preload and afterload, annulus dilation, and right ventricular systolic dysfunction (see Fig. 9). TR is frequently present in patients with mitral valve stenosis and severe TR has been found in about one-third of the patients after mitral valve replacement for rheumatic heart disease [69]. TR may result in significant symptoms, even advanced myocardial disease. For patients at high surgical risk, transcatheter tricuspid valve implantation/replacement (TTVI/TTVR) plays a significant role in the treatment of severe symptomatic TR (see Fig. 10). A few cases have been reported in patients with single-valve disease by the transjugular, transfemoral, or transatrial approach [70]–[73]. Similar procedures were performed for patients with multi-valve disease [74], [75]. In [76], Lauten et al. presented the first human case description of transcatheter treatment of severe TR in a 79-year-old patient with venous congestion and associated non-cardiac diseases. The treatment was performed by percutaneous caval valve implantation. The investigators in [75] described a successful TTVI procedure via the femoral route with very good results and no major complications for a 62-year-old man with severe TR due to bioprosthesis degeneration. The first human series of percutaneous tricuspid valve replacements in 15 patients with congenital or acquired tricuspid valve disease was detailed by Roberts et al. [77]. Procedural success was achieved in all 15 patients and their TR was reduced to mild or none. One case of third-degree
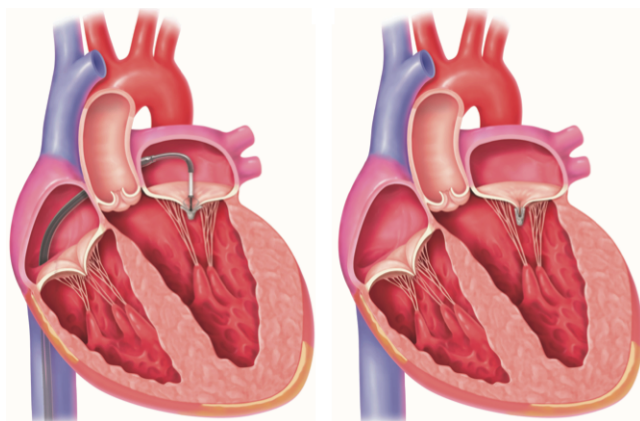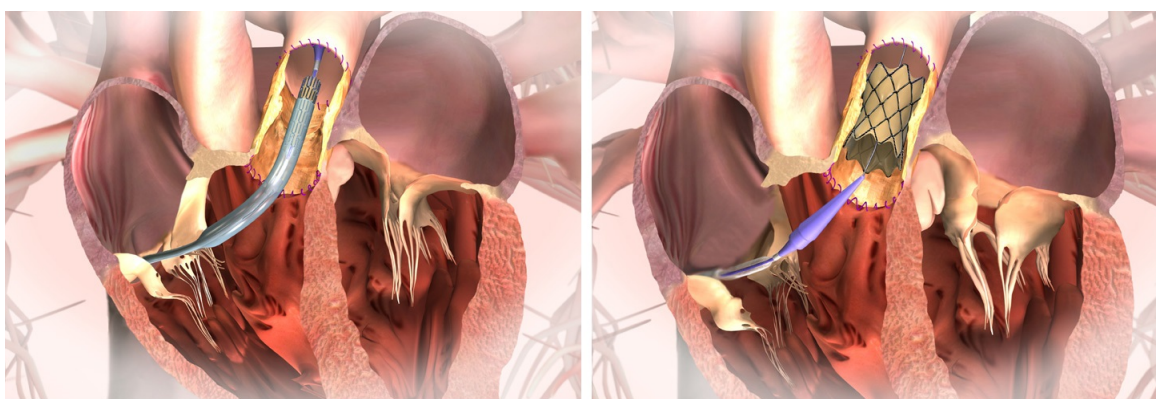
Fig. 8. The TPVR procedure through femoral artery (images are adapted from Medtronic [63]).
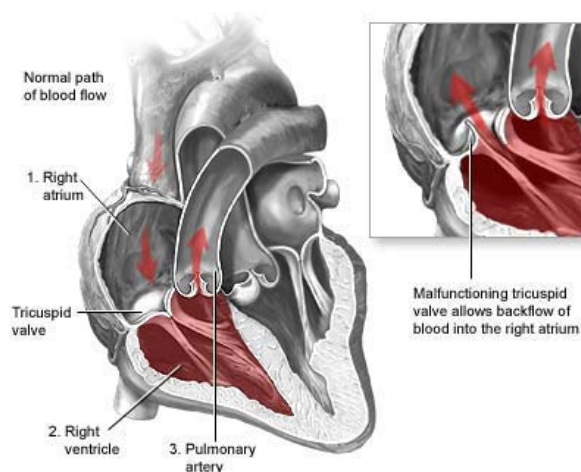

Fig. 9. Tricuspid regurgitation (image is adapted from Children's Heart Specialists [78]).

heart block was the only major complication, one case of endocarditis was found two months after implantation, and one patient with pre-procedural multi-organ failure died 20 days after the procedure. The other patients' bioprosthetic valves in the tricuspid position functioned well four months on average after replacement.

E. Transcatheter valve-in-valve implantation

Due to calcification or scar formation leading to valve dysfunction, the results of surgical valve repair or replacement are generally not very good and may result in bioprosthesis degeneration anywhere between 10-15 years after implantation [79]. Redo-valve surgery is challenging due to the fact that the patients are often in a poor clinical condition and it may cause more problems. Alternatively, transcatheter valve-in-valve implantation (see Fig. 11) is a promising treatment for high-risk patients with degenerated bioprosthetic heart valves [80]. The authors in [68], [81] described successful percutaneous implantations for aortic and pulmonary valves. Garsse et al. [82] presented the first successful percutaneous tricuspid valve-in-valve implantation for a 74-year-old patient with chronic obstructive pulmonary disease, severe stenosis of a degenerated tricuspid bioprosthesis, and other diseases.

In this case, an Edwards Sapien® 23 mm valve was placed inside a degenerated 25 mm Carpentier-Edwards bioprosthesis. In [83], Weich et al. reported a transjugular tricuspid valve-in-valve replacement for a 38-year-old woman with rheumatic heart disease. The patient's mitral valve prosthesis functioned well but her tricuspid prosthesis was severely calcified. Jux et al. [84] described the first successful percutaneous transcatheter double-valve-in-valve replacement in a single 26-year-old male patient via the femoral route, where two valves were implanted in the pulmonary and tricuspid position, respectively.

F. Transcatheter left atrial fibrillation ablation

Atrial fibrillation (AF) is the most common heart arrhythmia (see Fig. 12) and it is among the main causes of strokes. The transcatheter ablation procedure (see Fig. 13) is widely used for the treatment and cure of AF [86], [87], which is a minimally invasive surgery using high radio-frequency energy with a catheter from inside the atrium to eliminate the sources of ectopic foci, especially around the pulmonary vein (PV) ostia [88], [89]. The AF is finally removed by electrically isolating all the PV trunks of the left atrium (LA) from the rest of the heart using ablation. The complex and varying shape of the LA of different patients (e.g., size, position and number of PV ostia) [90] complicates this procedure. During the catheter ablation, CT or MRI imaging can be used to provide anatomical images of heart structures for the preoperative planning and intraoperative intervention.

Catheter-based ablation is very effective in the treatment of AF. However, this procedure could increase the risk of damage to the prosthetic valves in special patient groups. In [91], the authors described the safety, feasibility and efficacy of transcatheter ablation procedure in 26 patients with mitral valve prostheses (MVP). These patients had mitral valve surgery and subsequently developed AF, thus underwent circumferential PV ablation. To minimize the risk of valve damage during ablation, the catheter position relative to the valve and the leaflet motion were monitored by fluoroscopy. After a 3-month blanking period, they performed a 12-month follow-up, in which anti-arrhythmic treatment was considered for every subject. Compared with another matched group consisting of 52 ablated patients without MVP, the MVP group took a
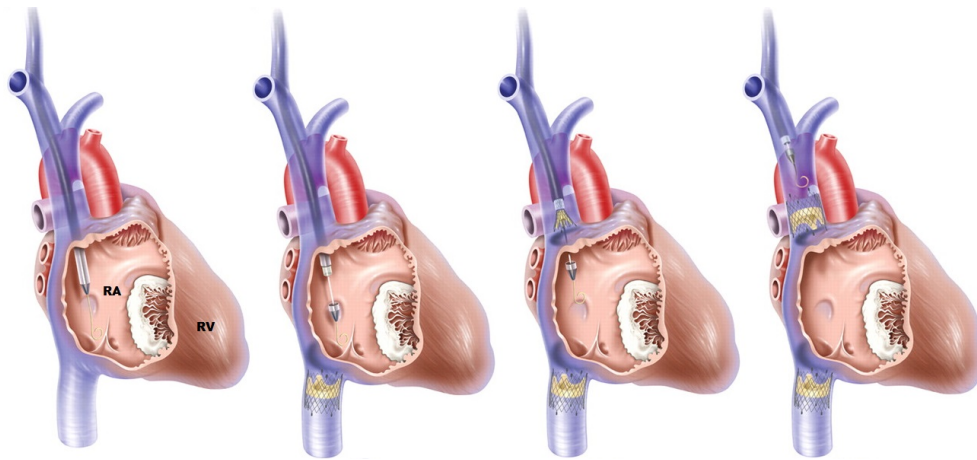
Fig. 10. The TTVI procedure [85] (RA: right atrium, RV: right ventricle).

much longer fluoroscopy time. At the end of follow-up, 73% of MVP patients were in sinus rhythm, slightly lower than the control group. Six patients in the MVP group had atrial tachycardia and three of them required repeat ablation, while only one patient in the control group had this problem and settled without treatment. No complications were found in control patients, while one femoral pseudoaneurysm and one transient ischemic attack occurred among MVP patients. The researchers concluded that AF ablation is feasible in MVP patients. More findings on arrhythmia and electrophysiology can be found in [92]–[95].

The AF may relapse following the transcatheter ablation. Manganiello et al. [99] investigated the incidence of symptomatic and asymptomatic AF recurrences applying continuous subcutaneous electrocardiogram (ECG) monitoring and insertable cardiac monitor (ICM, subcutaneously implanted during the ablation procedure) recording. They carried out a long-term follow-up of 113 patients who underwent PV ablation. According to the symptoms and ECG data, 40 patients demonstrated AF recurrences. Based on the ICM results, arrhythmia relapses were found in 75 patients (35 of them were asymptomatic).

Radio-frequency AF ablation has been widely practiced in many medical centers with numerous successes. However, complications like atrio-esophageal fistula could occur after
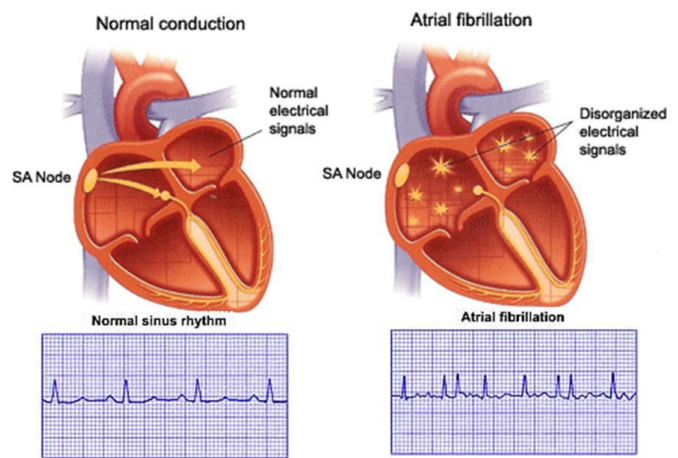
Fig. 12. Normal rhythm and atrial fibrillation (images are adapted from Healthy Habits Hotline [97]).
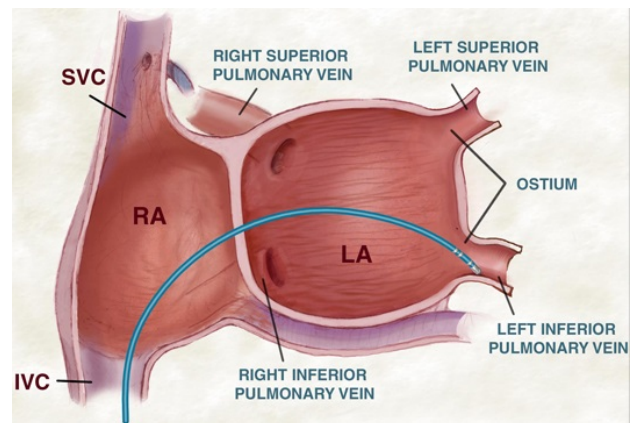
Fig. 13. Transcatheter left atrial ablation (image is adapted from Wellington Hospital [98]).
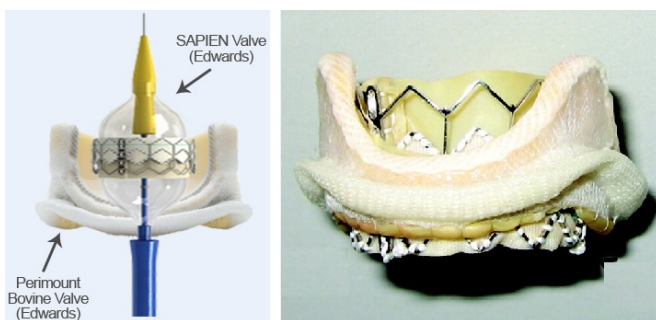
Fig. 11. The transcatheter valve-in-valve implantation procedure. (Left) A SAPIEN valve is deployed within a surgical Edwards prosthesis (image is from Heart Valve Surgery [96]), and (Right) a correct positioning where the SAPIEN valve overlaps the sewing ring of the surgical prosthesis [80].

this transcatheter ablation procedure in the posterior LA wall. Pappone et al. [100] reported two patients with cerebral and myocardial damage several days after undergoing circumferential PV ablation. One of them survived after emergency cardiac and esophageal surgery, and the other one died due to extensive systemic embolization. A recent case was presented

Fig. 14. Cross-sectional imaging of the arterial wall. (a) Four IVUS images acquired with transducers at different frequencies (green: media-adventitia border, red: lumen border) [8], and (b) an OCT frame (note the guide-wire shadow artifact at 'Guidewire') [102].

TABLE III
PHYSICAL CHARACTERISTICS OF CATHETER-BASED IMAGING (IVUS VS. OCT).

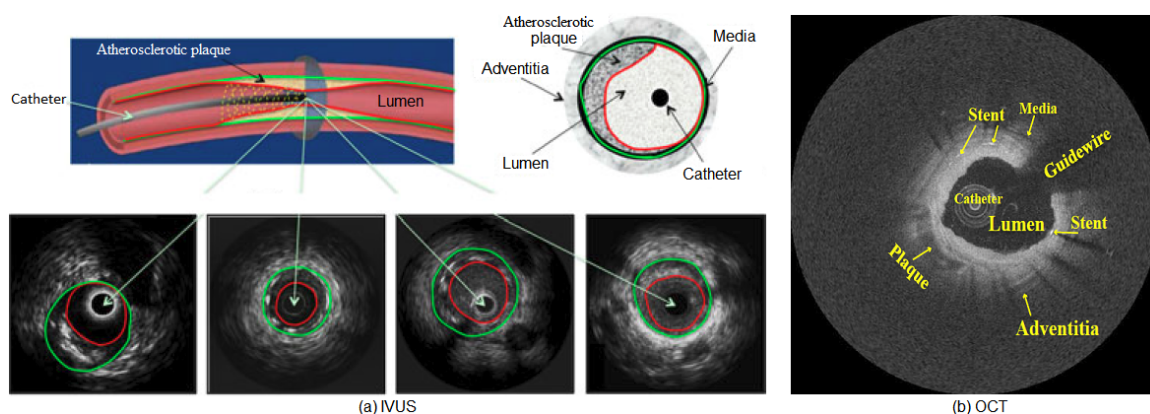| Property	IVUS	OCT
Energy source	Ultrasound	Near-infrared light
Wavelength (μm)	35-80	1.3
Frame rate (frames/s)	30	15-20
Pullback rate (mm/s)	0.5-1	1-3
Imaging resolution (μm)	Lateral: 200-300 Axial: 100-200	Lateral: 20-40 Axial: 15-20
Tissue penetration (mm)	10	1-2.5
Maximum scan diameter (mm)	15	7

in [101], where a 68-year-old woman presented bilateral oedema secondary to acute embolic stroke in the brain and air in the LA three weeks after transcatheter ablation for treatment of her chronic AF. Atrio-esophageal fistula was diagnosed in all of them.

G. Transcatheter technologies using IVUS and OCT

As a valuable complementary imaging modality to angiography, intravascular ultrasound (IVUS) and optical coherence tomography (OCT) have been widely used in coronary disease diagnosis and treatment. Compared to angiography that only depicts a 2D silhouette of the lumen, both modalities provide 2D cross-sectional images of the coronary artery vessel structure, assisting the clinicians in assessing the severity of a lesion, performing plaque classification, and determining the location and size for stenting.

IVUS is a catheter-based imaging technique, which places a catheter with a sensor on its tip inside the coronary artery (see Fig. 14a). The sensor rotates as it emits ultrasound pulses and receives echoes from the tissues around to generate tomographic images of the arterial wall in real time, which provides important information about coronary arteries including lumen, wall and plaque characteristics (e.g., shape and size). OCT is a novel intravascular imaging modality based on near-infrared light (shorter wavelength than ultrasound) emission, which enables a higher-resolution imaging of the arterial wall (see Fig. 14b) in the range of 10-20 microns than IVUS [103], [104]. Cross-sectional images are generated by measuring the echo time delay and intensity of light reflected or back-scattered from internal tissue structures [105]–[107]. In clinical

practice, IVUS and OCT can provide qualitative and quantitative assessment of coronary arteries and atherosclerosis. For example, OCT images can be combined with angiography to reconstruct the 3D coronary arteries for the evaluation of 3D arterial morphology [108], and the endothelial shear stress can be quantified using computational fluid dynamics of coronary arteries after 3D reconstruction for estimating the development and progression of coronary atherosclerotic plaque [109]. The authors in [110] analyzed a large number of intracoronary OCT images using a rapid and reliable segmentation algorithm, which can facilitate quantitative investigation of stent restenosis and thrombosis, as well as robust 3D reconstruction of coronary arteries to calculate endothelial shear stress in atherosclerosis. It also has potential application in plaque quantification and local hemodynamic analysis.

Table III shows the physical characteristics of IVUS and OCT [5], which are based on the Volcano, Boston Scientific, and Terumo IVUS systems and the Light Lab time-domain OCT imaging system that are commercially available. It is worth noting that OCT cannot image through a blood field which limits its adoption in clinical practice. In order to produce high-quality images, it requires clearing or flushing blood from the lumen during image acquisition. Both occlusive [111], [112] and non-occlusive [113], [114] techniques have been developed to stop the coronary blood flow during the acquisition period. The safety of intravascular OCT imaging mainly depends on the mechanical characteristics of the catheter and the extent of ischaemia caused by flow obstruction from the occlusion balloon when the occlusive technique is employed or the amount of contrast injected when the non-

TABLE IV
COMPUTER VISION TECHNIQUES INVOLVED IN TRANSCATHETER INTERVENTION.

Approach	Method	References
Gradient-based	1. Edge features	[9], [116]
	2. Radial grayscale gradient	[117]
	3. Radial grayscale gradient & variance	[118]
Statistical & probabilistic	1. Statistical shape driven	[119]
	2. Mixture of Gaussians	[120]–[123]
	3. Mixture of Rayleigh	[124]–[126]
Model-based	1. Active contour model	[127]–[130]
	2. Shape constrained deformable model	[131]–[139]
	3. Marginal space learning	[87], [140], [141]
Graph cut-based		[8], [11], [12], [142], [143]
Multiscale wavelet-based		[144]–[147]
Combined		[148], [149]
Applications	1. Annulus measurement	Imaging-based [42], [150], [151]
		Robot assisted [152]–[154]
		Ring fitting [155]
	2. Ventricle segmentation	Graph search [156]
		Dynamic programming [157]
		Combined [158], [159]
		Atlas-based [160]
		Active shape model-based [161]–[163]
	3. Atrium segmentation	Model-based [87], [139], [141], [164]–[166]
		Non-model-based [86], [167]
	4. Vessel centerline extraction	Border detection [168]–[170]
		Vessel tracking [171], [172]
		Active contour model [173]
		Minimum distance [174], [175]

occlusive technique is applied. OCT imaging technique has been considerably adopted across Europe and Japan, though not approved in USA yet. Preliminary studies of patients with coronary artery diseases using both occlusive and non-occlusive techniques show that the OCT image acquisition is safe and no major complications occurred [113], [115]. Compared to IVUS, OCT provides superior visualization and differentiation of the lumen and arterial wall interface, which facilitates the determination of lumen areas and volumes [5]. Due to a low crossing profile, the OCT imaging wires are able to negotiate tight lesions that the IVUS catheter is unable to cross and it can also measure smaller lumen sizes than IVUS [115]. Because of its limited tissue penetration ability, OCT may not be suitable for investigating vessel remodeling, which is well addressed by IVUS.

III. COMPUTER VISION TECHNIQUES IN TRANSCATHETER INTERVENTION

Transcatheter intervention is an interdisciplinary technique, involving clinical, imaging and interventional surgeons, cardiologists, radiologists and anesthesiologists. Appropriate image processing and analysis, real-time interactive segmentation, and visualization tools can help them to cooperate and communicate efficiently to find an optimal treatment for a patient. Moreover, preoperative and intraoperative imaging provides a large amount of volumetric images for the planning and guidance of the transcatheter intervention. To make use of these data for clinical investigations, precise measurement of the geometric features (e.g., diameter, center and orientation of the aortic valve annulus) and accurate segmentation of

the anatomical structures (e.g., left ventricle and left atrium) are essential. In this section, we concentrate on those state-of-the-art computer vision techniques that have been widely applied in the minimally invasive transcatheter procedure (see Table IV).

A. Gradient-based approaches

The edge patterns in IVUS images can be used to distinguish lumen and media-adventitia contours. Hybrid algorithms have been developed to incorporate such edge features into desirable target boundaries. These techniques usually require precise initialization and rely on energy minimization. An early work was introduced by Sonka et al. [9] for the detection of internal and external elastic laminae (inner and outer media layers) and plaque-lumen borders. After removing the calibration markers and selecting the regions of interest (ROIs), the authors applied Sobel-like edge detectors on subimages to construct laminae and lumen border graphs and then performed heuristic graph search deploying two distinct cost functions to detect the borders. In this work, dynamic programming is used to search a minimum path in the cost function, which incorporates edge information with a simplistic prior, based on echo pattern and border thickness. The presented technique demonstrated good correlation between manually and automatically detected lumen borders, plaque areas, and percent area stenoses. However, it requires manual initialization. An extended version of this approach using a different cost function and 3D optimal graph search was presented in [116], where the authors applied principal component analysis (PCA) to reduce the noise and increase the homogeneity of intensity within the ROIs, and
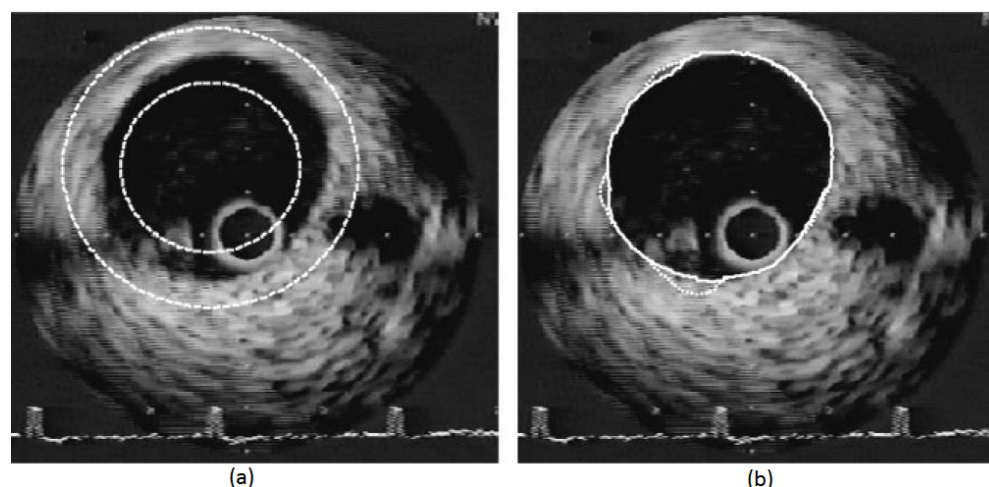
Fig. 15. A typical contour detection result. (a) Initialized annular region in an IVUS image, (b) Obtained contours using ordinary (dotted) and modified (solid) methods [118].

then estimated the initial lumen border by applying a spline-based active contour model for the following graph-search segmentation.

In [117], Meier et al. proposed to automatically segment both lumen and media-adventitia boundaries through the enhancement of image continuity along the circumferential direction in polar coordinates and speckle noise reduction using iterative nonlinear spatial median filters. They applied three different segmentation methods for the detection of the lumen borders: i) thresholding of radial grayscale gradient maps obtained by convolving the polar image with gradient kernels, ii) adaptive region growing from a luminal seed point after detecting the catheter outline, and iii) deformation of a gradient-based parametric deformable model to search for connected outline points and detect the media-adventitia border. In addition, postprocessing involving dropout filtering and outline smoothing is required to remove remaining outliers and refine the final segmentation. Two data sets of 77 and 28 IVUS images of human coronary arteries are selected for the identification of lumen and media-adventitia borders, respectively. Experimental results show that the first strategy is robust and outperforms the other two approaches, while they are more computationally intensive. Instead of using image gradient only, Luo et al. [118] designed a modified cost function combining both gradient and variance of the grayscale intensities in the radial direction, which is less sensitive to noise. They employed circular dynamic programming to extract the media-adventitia boundaries. It has been demonstrated that the presented algorithm can attain high accuracy and reliability in the measurement of the lumen area variation (see Fig. 15). However, manual initialization of the ROI and the origin point in the first frame are required.

To improve the convergence capability of existing methods, Xie and Mirmehdi [176] proposed an external magnetic vector force field based on hypothesised magnetic interactions between the image gradients (object boundary) and active contour. It can attract the contour to deep concave regions, without suffering from saddle point and stationary point problems. This image gradient based assumption was later extended to 3D medical image segmentation [177].

B. Statistical and probabilistic approaches

Border detection and region identification in IVUS coronary artery images are challenging tasks. Few algorithms have been developed in order to trace the intima and the media-adventitia automatically. Statistical approaches are generally proposed based on an assumption that grayscale values corresponding to lumen and plaque (intima) regions are generated by two distinct distributions that can be modeled parametrically [125] (e.g., Rayleigh or mixture of Gaussians) or non-parametrically [119]. Taking advantage of this property, Gil et al. [120], [121] suggested the use of elliptic templates guided by the global statistics inside regions to model and detect the lumen borders of coronary arteries for the first time. They incorporated two different Gaussian probabilities corresponding to lumen and tissue areas into a deformable model with elliptical shape constraint. The use of probabilities can reduce the impact of speckle noise in low-quality IVUS images, while the restricted deformable shape makes the model more robust to shadows due to calcium plaque and artifacts of the catheter. Similarly, Taki et al. [123] developed an automatic approach for the identification of the intima and the media-adventitia borders simultaneously using two different thresholds after despeckling through affine invariant anisotropic diffusion filters.

In practice, the vessel border detection is a complex problem, requiring sophisticated methods. By assuming a Rayleigh distribution and modeling the expected contour with a priori knowledge using Markov processes, Haas et al. [124] incorporated additional information about the speckle appearance. The final contours were automatically extracted by applying a maximum a posteriori (MAP) estimator iteratively. The algorithm was tested on 29 *in vivo* frames and achieved satisfactory results. Similarly, the authors in [125] introduced a fully automatic method to estimate the luminal contour in intra-coronary ultrasound images using a MAP estimator and a constraint on the first zero crossing of image derivatives on the borders. The image brightness appearance was modeled by a
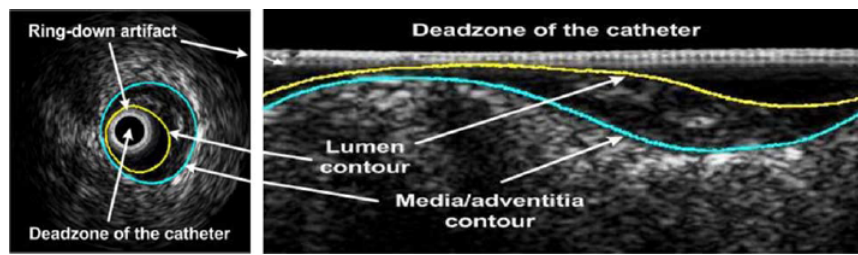
Fig. 16. Lumen and media-adventitia contours of an IVUS image in the original and rectangular domains [119].
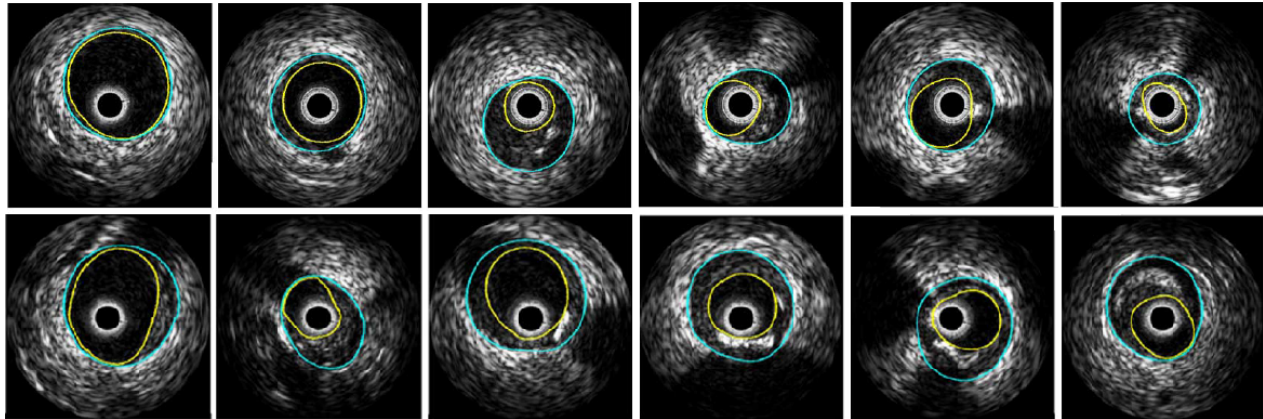

Fig. 17. Examples of lumen and media-adventitia contours: (Top) without feature extraction for cases with no/minor calcifications and branch openings, and (Bottom) with feature extraction for cases with calcifications and branch openings [119].

Rayleigh distribution. In [126], Cardinal et al. developed a 3D segmentation model for IVUS pullback image volumes based on the fast-marching framework [178] and applying a mixture of Rayleigh distributions modeling the gray level probability density functions corresponding to the vessel wall structures. The regions were initialized using manually traced lumen and media borders in several frames on longitudinal image cuts. The proposed algorithm was evaluated using different initializations on 9 *in vivo* IVUS pullbacks of superficial femoral arteries and a simulated volume. They obtained accurate results on simulated data with small average point-to-point distances between detected vessel wall borders and ground truth. On *in vivo* IVUS volumes, a good overall performance was achieved with acceptable average distance between segmentation results and manually traced contours. Likewise, a 2D semi-automatic technique was presented in [122] using a parameterization of the lumen region with a mixture of Gaussian distributions. The lumen border was finally detected by minimizing a cost function that linearly combines the steepest descent technique and the Broyden-Fletcher-Goldfarb-Shanno (BFGS) method [179], resulting a faster convergence toward a global minimum.

The assumption of grayscale intensities in IVUS images satisfying parametric Rayleigh or Gaussian distributions may not be true in all situations. Alternatively, Unal et al. [119] proposed an automatic shape-driven approach for the segmentation of arterial wall boundaries from IVUS images in the rectangular domain (see Fig. 16). They first built a statistical shape space using PCA and then evolved an initialized contour from the surface of the transducer in polar coordinates by minimizing a region-based non-parametric probabilistic energy

function. The probability distribution inside and outside the lumen was estimated by using intensity profiles from a training data set. The lumen borders were automatically extracted, while the media-adventitia (MA) borders were detected using edge information instead to evolve the curve. The performance evaluation on a large data set demonstrated the effectiveness of the presented technique. Fig. 17 shows several examples of detected lumen and MA contours.

C. Model-based approaches

Due to the limited image quality (e.g., low contrast) of the volumetric data acquired during the transcatheter procedure, model-based approaches may be most appropriate for the segmentation of anatomical structures containing in these volumes. To improve the robustness of segmentation, model-based methods exploit the prior knowledge such as shape information to guide the image segmentation process. With the prior constraints, the model-based segmentation can avoid leakage around weak or missing boundaries. However, it may be difficult for them to handle the structural variations.

1) Active contour models: Active contour models (snakes) have been widely used in many medical image segmentation applications, which represent contours or surfaces in their parametric form during deformation. The main idea is to place an approximate contour close to the desired features in an image and then allow the contour to deform under the influence of external and internal forces in the energy function to snap to the desired features. The external force pushes the contour toward the desired image features, while the internal force ensures that the contour maintains its overall shape and
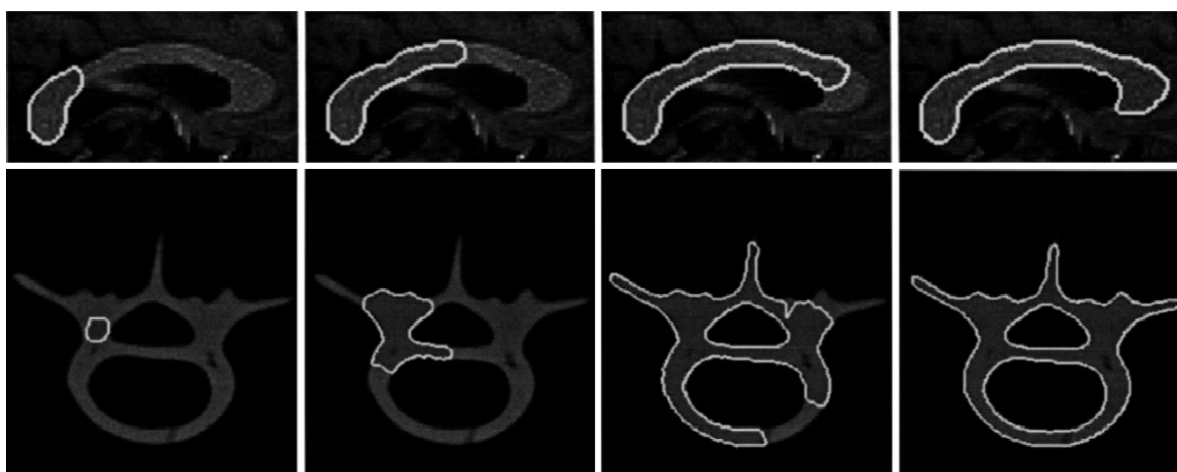
Fig. 18. Segmentation process using topology adaptive snakes: (Top) a corpus callosum from MRI brain image slice, and (Bottom) a cross-sectional images of a human vertebra phantom [180].

continuity in the process. The deformation stops when the forces balance each other and the contour no longer moves significantly. Fig. 18 gives two examples of the deformation process, illustrating the high flexibility of snakes. The contour models are able to track the points on the curves or surfaces across time, and are suitable for real-time applications. However, they generally have difficulties in handling topological changes due to the parameterization of the curves or surfaces.

The traditional parametric snake models [127], [128] are popularly adopted for the segmentation of IVUS image data [8]. Rather than implicit shape surface representation to retrieve lumen and media-adventitia boundaries, parametric model formulation is more intuitive since the topology of different boundaries is simple and underlying parameterization remains simple and computationally efficient. However, it relies on good initialization and fine parameter tuning. Generally, the vessel borders in IVUS images are not well distinguished, which hinders the application of the classical snake models. Hence, preprocessing techniques (e.g., nonlinear filtering [181]) or energy optimization skills (e.g., Hopfield neural network [182]) are incorporated prior to the use of the snake framework. By modifying the terms of the energy function, several approaches have been proposed to detect the lumen and media-adventitia borders. Shekhar et al. [129] developed an active surface model for the identification of both borders. In this 3D segmentation algorithm, an initial surface template is placed close to the desired arterial wall and then deformed to snap to it according to the external, internal and damping forces. The external force is the gradient of a 3D potential field computed by convolution of the image volume with three 3D Sobel-like kernels, which draws the vertices of the template towards the desired arterial border. The internal force is based on the transverse and longitudinal curvature vectors in the local radial direction, which maintains the smoothness of the surface model. The damping force is used to help the model to converge to its final shape. The presented technique is statistically accurate, robust to image artifacts, and capable of segmenting volumetric IVUS images rapidly. It enables geometrically accurate 3D reconstruction and visualization of

coronary arteries and volumetric measurements. In addition, it can be applied to segment 3D images of other modalities. Nevertheless, the algorithm requires user intervention to place an initial contour every ten slices. To automatically identify the lumen and media-adventitia borders, Kovalski et al. [130] proposed a 3D segmentation approach. The elasticity term in the snake framework [127] is removed from the internal energy. To control the contour smoothness, they introduced a priori on the final desired shape through regularization along the longitudinal direction, and a balloon force to control the point motion along the radial direction. Compared to manual tracing of both borders, the automatic results demonstrates high correlation and low variability, which indicate that the suggested method may potentially provide a clinical tool for accurate lumen and plaque assessment.

To make the geometric snake model more robust to weak edges and noise in medical images, the authors in [183] integrated the gradient flow forces with region constraints. An alternative approach to this hybrid image force can be found in [184], [185], where Jones et al. combined the edge-based and region-based constraints with graph cut and superpixel for interactive segmentation of the MA border in IVUS images and lumen border in OCT images. Compared with other approaches, this combinatorial method demonstrated improved versatility and better segmentation results. To deal with more complex topological changes and enable free initialization of contour/surface in the image, Xie and Mirmehdi [186] introduced the radial basis function interpolated level sets into the region-based active contour model. Unlike traditional level set based schemes, the proposed implicit active model does not require periodic re-initialisation and allows coarser computational grid, leading to great potential in modelling in high-dimensional spaces.

2) Shape constrained deformable models: Among many others, active shape models [131]–[133] are fast and robust, where the object shapes are represented by a point distribution model [131], [132] or a hierarchical parametric descriptor [133]. However, the segmentation accuracy is limited because the deformations of these models are restricted by a

few statistical parameters of training samples. Furthermore, a large training set is required to build a representative shape model. Elastically deformable models [134], [135] are more flexible and provide a straightforward way to involve prior information for image segmentation by incorporating prior statistics to constrain the variation of the model parameters. However, the initialization is critical, which often needs to be very close to the object contour to produce good segmentation results. This is due to the presence of disturbing attractors in the image, which do not belong to the object of interest, but force the models towards undesired object boundaries. To overcome difficulties and take advantage of both approaches, Weese et al. [136] embedded an active shape model into an elastically deformable surface model, where the shape model restricts the flexibility of the surface mesh and maintains an optimal distribution of mesh vertices. Adaptation to the image boundaries is controlled by an external energy derived from local surface detection and an internal energy that constrains the deformable surface to stay close to the subspace defined by the shape model. The internal energy is defined with respect to the shape model, where the pose and parameters of the shape model are adapted together with the mesh vertices representing the deformable elastic model. Moreover, the external energy has been designed to reduce the risk that the mesh is trapped by false object boundaries, as it attracts the deformable model to locally detected surfaces. Such a shape constrained deformable model can capture anatomical structures even though they cannot be exactly described by the model, as it is not restricted to the subset of modeled shapes. In [187], Yeo et al. proposed a novel variational approach for level set segmentation with statistical shape prior. By applying kernel density estimation, the incorporated shape information enables the described model to efficiently handle complex shapes from occluded and noisy images.

To segment the left atrium and pulmonary veins (LAPV) in the rotational X-ray angiography images for the transcatheter atrial fibrillation ablation procedure, Manzke et al. [139] presented an automatic model-based segmentation algorithm, where the anatomical prior knowledge is encoded within a geometric LAPV shape model. This technique is based on the shape-constrained deformable models [136] and follows the general framework in [137] with several extensions: i) the LAPV model is based on the four chamber model [137] with extension of the major vascular structures [138], ii) the detection of the left atrium with the generalized Hough transform has been slightly modified and takes only boundaries with distinct gray value properties in a $3 \times 3 \times 3$ neighborhood into account, iii) a histogram-based calibration method is used to reduce intensity variations between images, and boundary detection is performed on calibrated gray-values, iv) the progressive adaptation technique introduced in [138] for the adaptation of major vessels attached to the heart is used to segment the pulmonary veins, and v) some aspects of the generation of the reference meshes are specific for the presented LAPV surface generation.

As shown in Fig. 19, shape constrained deformable models can be used for the segmentation of various anatomical structures such as vertebra, femur, aorta in CT images [136],

and LAPV surface in 3D rotational X-ray angiography images [139].

3) Marginal space learning: In many applications, instead of uniform and exhaustive search, the posterior distribution can be clustered in a small region in the high-dimensional parameter space. For example, in 2D space search, a classifier trained on $p(y)$ can quickly delete a large portion of the search space, and the classifier for joint distribution $p(x, y)$ can then be trained in a much smaller region (see Fig. 20a). Based on this observation, Zheng et al. [140] proposed marginal space learning (MSL), an efficient method to search such clustered parameter spaces. The idea of MSL is not to learn a classifier directly in the full similarity transformation space but to incrementally learn classifiers on projected sample distributions. In MSL, the dimensionality of the search space is gradually increased, e.g., a 3D object localization problem can be split into three steps: position estimation, position-orientation estimation, and position-orientation-scale (full similarity transformation) estimation. After each step, only a limited number of candidates are reserved to reduce the search space. To further improve the efficiency, a pyramid-based coarse-to-fine strategy can be applied.

The MSL has been successfully demonstrated on many medical image segmentation problems. To quantitatively analyze the heart function from 3D cardiac CT volumes, Zheng et al. [140] developed an efficient and robust approach for automatic four-chamber heart segmentation (see Fig. 20), which consists of two steps: anatomical structure localization and boundary delineation. In this work, the MSL algorithm is first employed to solve the 9D similarity transformation search problem for automatic heart localization. After determining the pose of the heart chambers, a learning-based 3D boundary detector is then applied to guide the non-rigid heart shape deformation. To handle the structural variations and obtain robust performance on emerging C-arm CT images, Zheng et al. [141] proposed an automatic model-based method for the left atrium (LA) segmentation. Instead of using a holistic mean shape model [139], the authors applied a multi-part-based model to address the variations in pulmonary veins (PVs), which splits the whole LA into six parts: chamber body, appendage and four major PVs (left inferior, left superior, right inferior, and right superior). Compared to the mean shape model in [139], each part has a simpler anatomical structure that can be detected and segmented well using MSL. After segmentation, all the six parts are then merged into a consolidated mesh, with different anatomical structures labeled by different colors. However, it is still hard to accurately segment the connection region to the LA chamber (the region around the PV ostia and appendage). To overcome this shortcoming, Zheng et al. [87] suggested a way to precisely segment the ostia region by enforcing both the image boundary delineation accuracy and mesh smoothness.

D. Graph cut-based approaches

The catheter-based imaging techniques such as IVUS and OCT provide 2D cross-sectional images of the coronary artery. Accurate segmentation of the inner/outer arterial wall in these
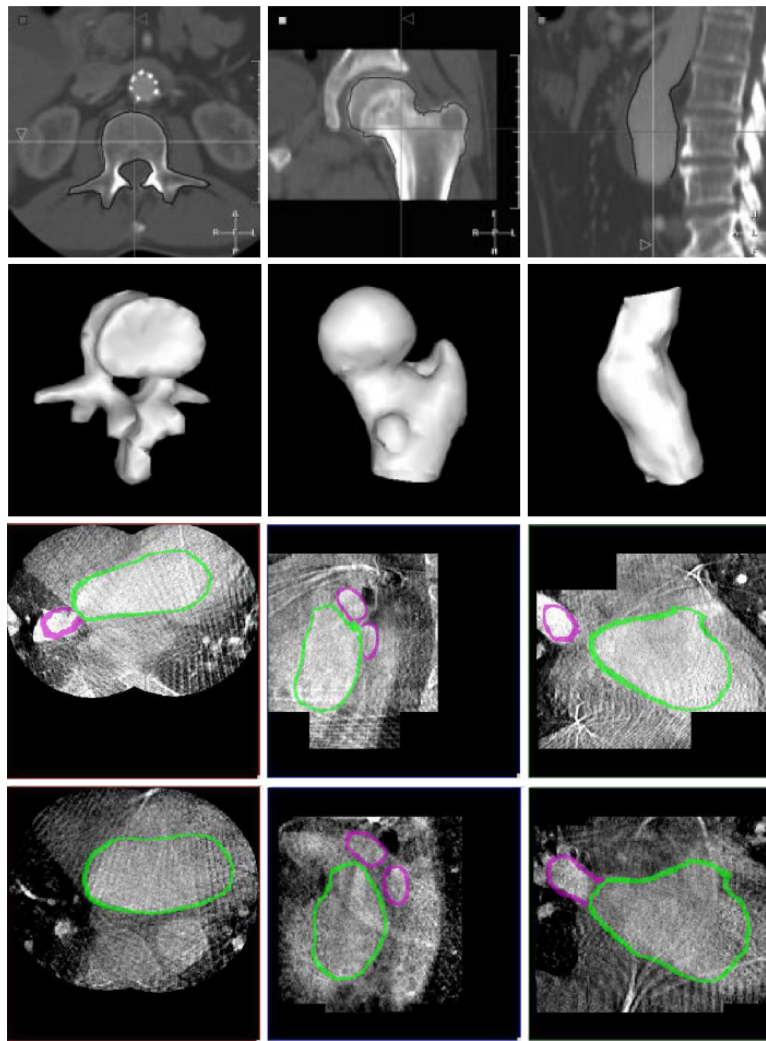
Fig. 19. Segmentation results of (Top) vertebra, femur, aorta in CT images [136], and (Bottom) 3D rotational X-ray angiography data of two patients in (from left to right) axial, sagittal, coronal views [139].
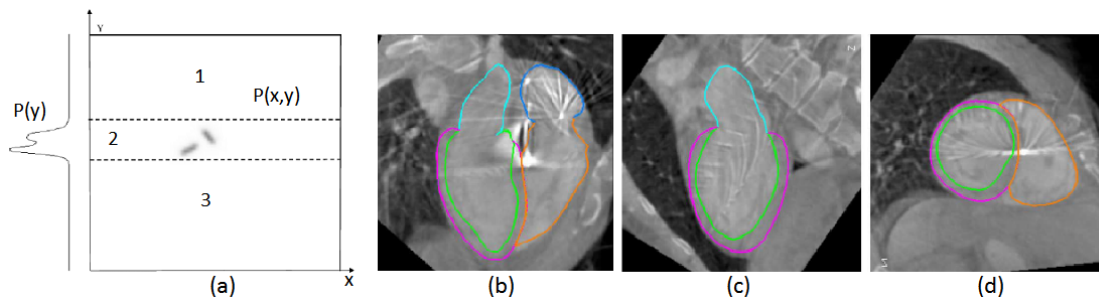

Fig. 20. MSL-based segmentation of 3D cardiac CT volumes. (a) MSL, and (b-d) extracted heart chamber in axial, sagittal, coronal views with green for LV endocardium, magenta for LV epicardium, cyan for LA, brown for RV, and blue for RA [140].

images is a prerequisite for clinical investigations, which provides critical information for coronary disease diagnosis and treatment. Among many others, graph cut-based approaches [8], [11], [12] have shown to be very promising for the segmentation of IVUS images.

In [142], Wahle et al. applied the novel s-t cut algorithm [188] (see Fig. 21) to segment 3D IVUS images, where the cost function used for identifying the lumen-plaque and media-adventitia (MA) surfaces contains three-tiered information at both global and local levels: intensity patterns along the borders, Rayleigh distribution of ultrasound image data, and regional homogeneity based on Chan-Vese minimum variance criterion. However, these intensity-based features are susceptible to IVUS image variations such as calcification and shadow. Based on the efficient graph construction method presented in [143], Essa et al. developed an initialization-free approach for automatic extraction of MA border in IVUS images using double-interface graph cut segmentation [11]. The images are first transformed from Cartesian coordinates to polar coordinates, which removes the catheter regions and transforms a closed contour segmentation into a 'height-field' segmentation. This transformation facilitates the construction
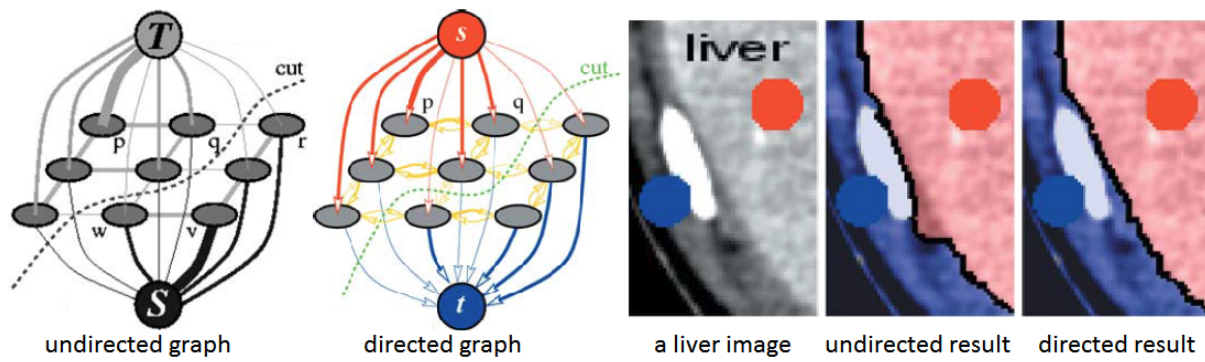
Fig. 21. Graph cut-based segmentation of a liver image on an undirected graph and a directed graph (a cut divides the nodes between the source terminal *S* and sink terminal *T* that represent 'object' and 'background', respectively) [188].
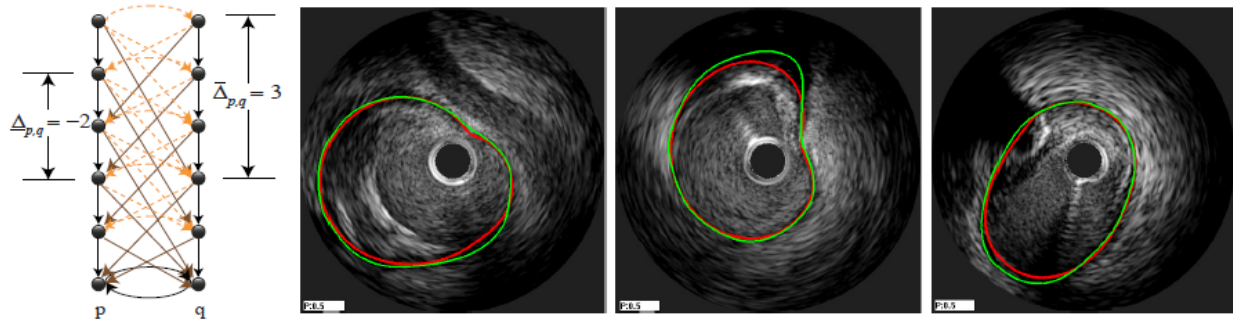

Fig. 22. Automatic segmentation of IVUS media-adventitia borders on a directed graph with shape priors (green: ground truth, red: proposed method) [11], [12].

of an arc-weighted directed graph, on which a minimum s-t cut can be computed without any user initialization. The authors applied the arc-weighted directed graph construction to impose geometrical and smooth constraints learned/derived from the generalized shape priors [12] of multiple training shapes, and built novel cost functions using a combination of complementary texture features. Fig. 22 shows a qualitative comparison between the manually labeled results and those by Essa's method [11].

E. Multiscale wavelet-based approaches

Taking advantage of spectral analysis or spatial-frequency expansions, Katouzian et al. [144] introduced the first multiscale expansion approach based on discrete wavelet packet frames to automatically detect the lumen borders in IVUS images. First, the images are decomposed onto orthogonal Lemarie-Battle filters and the envelope of the complex coefficients is then computed as features. An unsupervised K-means clustering algorithm is applied to generate binary masks corresponding to blood and non-blood regions. The lumen border is evaluated by iterative Spline interpolation among nearest detected edge sets in the radial direction. However, the presence of the guide wire, ring-down artifacts, and attenuation of signals in regions far from the transducer limits the proposed method. Similarly, the authors in [145] applied the discrete wavelet frames to identify both the lumen and MA borders in IVUS images, where the decomposition trees were constructed by the Haar filters (see Fig. 23). Both

techniques are able to automatically delineate borders with four decomposition levels in polar coordinates.

Motivated by the procedure used by interventional cardiologists, Katouzian et al. [146], [147] developed an automatic technique to trace the lumen borders in IVUS images acquired with high-frequency transducers. IVUS subvolumes were projected onto orthogonal brushlet basis functions in an overcomplete fashion in polar coordinates, as the brushlet coefficients are invariant to intensity and only depend on the spatial frequency content of the IVUS signals. In this work, two approaches were proposed for the estimation of the lumen border. They binarized the brushlet coefficients by assuming that those corresponding to plaque regions have higher magnitude, and then applied the iterative conditional model segmentation framework with Markovian regularization to identify the lumen borders in different classes [146]. The evaluation on *in vitro* data demonstrated that distinct histogram peaks correspond to blood and non-blood regions. Thresholding of these peaks leads to binary masks exploited for the detection of the lumen border with the surface function active framework. In addition, techniques for removing catheter marker, ringdown, and guide wire artifacts were introduced as well.

F. Combined approaches

The combination of different segmentation approaches (e.g., model-based and graph cut-based methods) can take advantage of them to produce better results or more anatomical structures, which is potentially helpful for medical diagnosis,
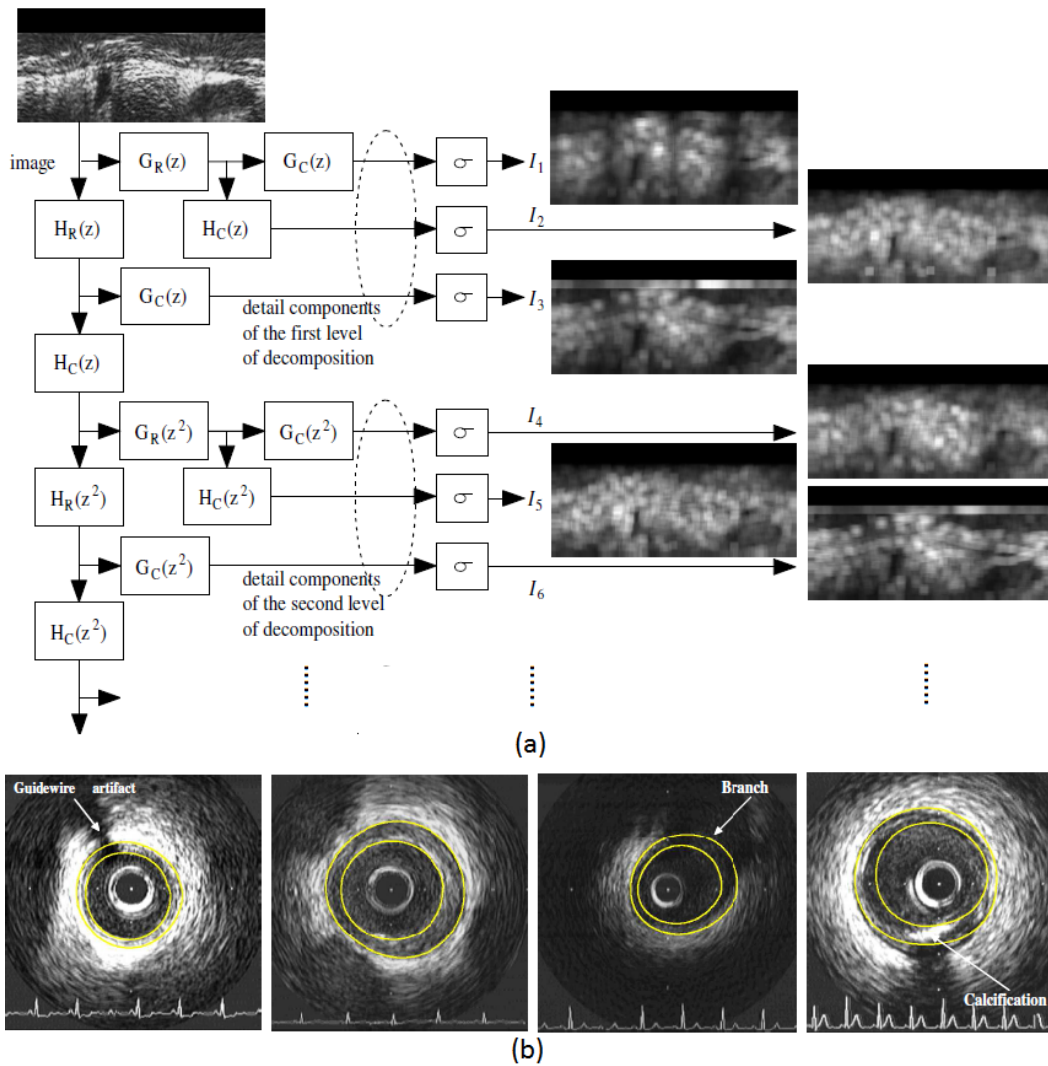
Fig. 23. Automatic IVUS contour detection. (a) Fast iterative 2D discrete wavelet frames decomposition of four levels (only two levels are shown), the input IVUS image is in the polar coordinates (rectangular domain), R and C denote filters applied row-wise and column-wise respectively, and (b) segmentation results of different images [145].

preoperative planning, and intraoperative guidance during the transcatheter procedures.

Zheng et al. [87], [141] developed a robust and efficient model-based method to automatically segment the LA from 469 C-arm CT volumes using MSL. However, on some image data, the final consolidated mesh may slightly deviate from the true LA boundary since the method does not make full use of local voxel-wise intensity information. Furthermore, due to the large variations of the PV drainage pattern, the extra right middle PVs between two major right PVs are not included in the multi-part-based LA model, although these anatomies are important for cardiac diagnosis and treatment planning. To refine the LA segmentation and extract the right middle PVs, Yang et al. [149] proposed an automatic approach combining the model-based method with graph cut-based method (see Fig. 24). Based on the initial segmentation results by the model-based approach, two regions of interest (ROIs) are first determined for the LA segmentation refinement and right middle PVs extraction, respectively. The initial segmentation also provides positive (foreground) and negative (negative)

seeds to automatically initialize the graph cuts. The graph is then constructed within the corresponding ROI by a region growing process, which connects the seeds and voxels of ROI together without duplication. By performing the graph cut optimization, the voxels within the two ROIs are relabeled as foreground and background. The foreground voxels are used to update the initial segmentation and refined segmentation results. To reduce the leakage of graph cuts for the extraction of right middle PVs, a pruning procedure is exploited to remove occasional false positive PVs by examining multiple criteria. Finally, the initial segmentation is refined and further expanded with newly detected right middle PVs. Fig. 25 shows the final extraction results of the LA and right middle PV.

To automatically detect the MA border, Gil et al. [148] combined a statistical strategy with a supervised classification approach to achieve optimal performance. The presented segmentation method consists of three main steps. First, a restricted anisotropic diffusion filter is applied to enhance the border. Second, a feature space consisting of horizontal edges, radial standard deviation, and radial cumulative mean is
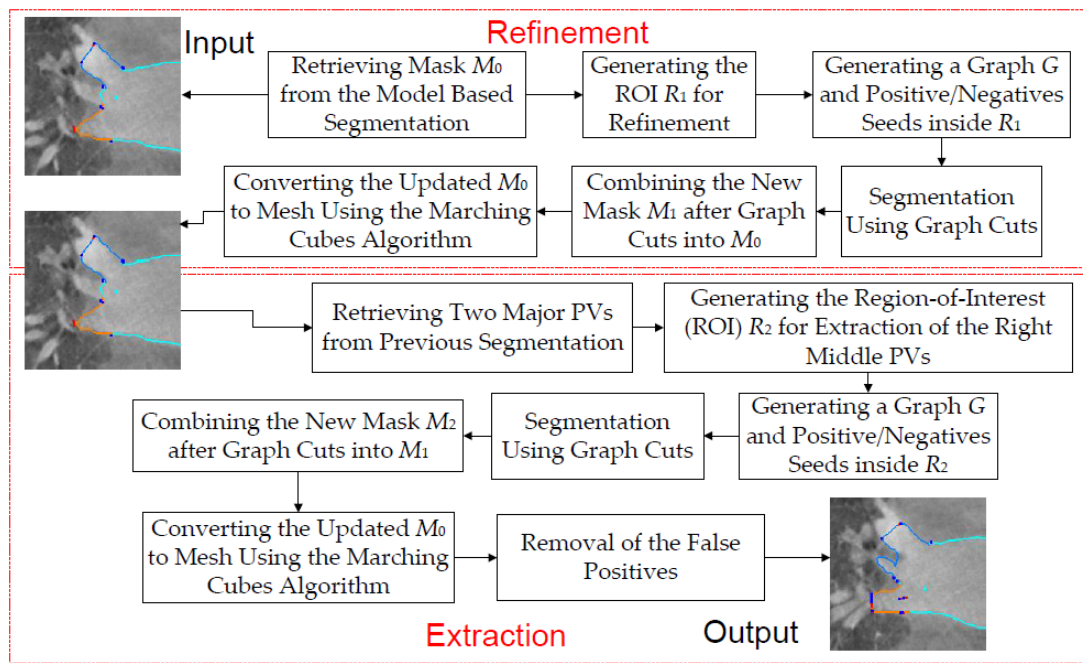
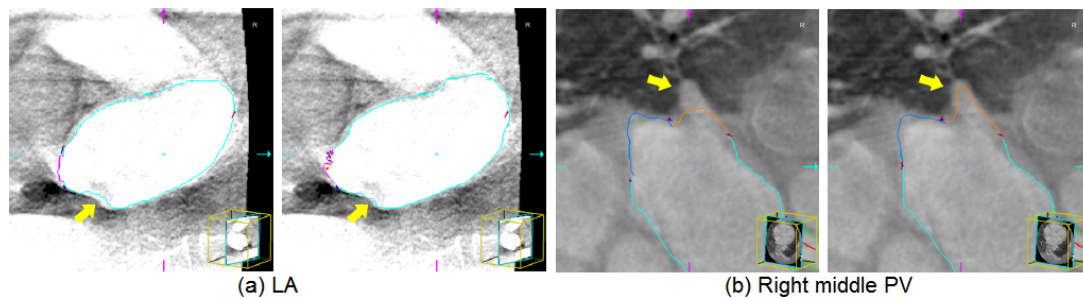Fig. 24. The flowchart of Yang's combined approach [149].

Fig. 25. Segmentation results of (a) LA and (b) right middle PV. The small defect of LA and non-detected right middle PV (yellow arrows) in the model-based segmentation (odd columns) are corrected after refinement (even columns) [149].

constructed. The edge feature represents the MA border, while the other two features can be used to differentiate between calcified and fibrotic tissue within the plaque. Fisher linear discriminant analysis (LDA) is then performed to achieve a maximum separability among the projected classes followed by Bayesian thresholding in the feature space to generate two binary masks corresponding to calcified regions and the MA border, respectively. Third, the MA border is identified through modeling the fragmented segments in the MA border mask by computing an implicit closed representation using an anisotropic contour closing and an explicit B-spline compact parameterization.

In conventional sequential approaches, segmentation and interpolation are carried out separately in turn. Some methods first perform segmentation of the slices and then interpolate a 3D surface from the segmented 2D contours, while other methods perform interpolation of the slices first to reconstruct a 3D volume, followed by 3D segmentation. Both of them have limitations in processing 3D and 4D sparse medical data sets. In [189], Paiement et al. accomplished both segmentation and interpolation simultaneously by integrating them into a radial basis function (RBF) interpolated level set framework,

which combines the flexibility of level set methods, the numerical stability of RBF interpolated level set segmentation methods, and the interpolation abilities of RBFs. In this work, the interpolation exploits the segmenting surface and its shape information instead of pixel intensities, thus achieved improved robustness and accuracy. Moreover, the proposed method supports any spatial configurations of 2D slices with arbitrary positions and orientations.

G. Applications

In this section, we review some of the computer vision techniques applied in transcatheter interventions with respect to applications, such as the measurement of aortic valve annulus for valve selection in TAVI, detection of ventricle and atrium for assessing the heart functional and guiding the intraoperative procedure, extraction of vessel centerline in coronary angiographic images for estimation of vessel parameters, and so on.

1) Annulus measurement: The success of TAVI highly depends on proper preoperative planning and accurate intra-operative valve placement. During preoperative planning of
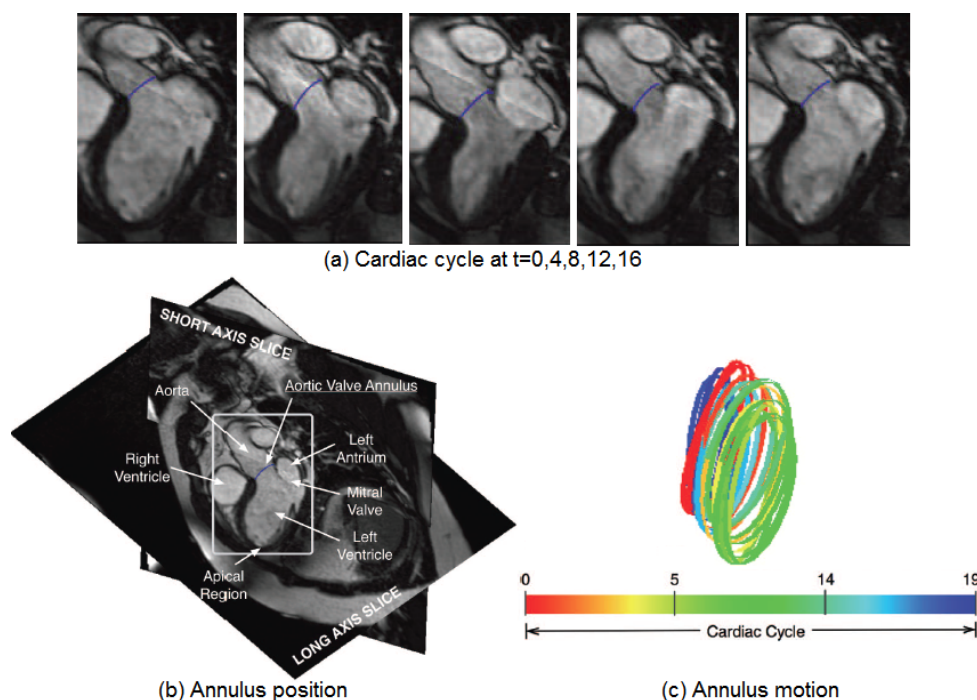
Fig. 26. Measurement of the aortic valve annulus (blue curve). (a) Annulus tracking in 5 (out of 20) frames at selected instances over a complete cardiac cycle, (b) annulus position with respect to short and long axis slices for one frame, and (c) color-coded annulus positions at different instants in one cycle [155].

valve implantation, one of the major steps is to determine the prosthetic valve size and type based on the accurate measurement of the geometric features of the aortic valve annulus including its diameter, center and orientation (the direction along which the prosthetic valve can be deployed). Generally, these features can be estimated by ultrasound or X-ray based imaging technologies such as TTE, TEE and multislice CT [151]. MRI can be used for evaluating the annulus features during the preoperative planning as well as tracking its motion during TAVI to guide the valve placement [42], [150]. Robotic assistance can also be integrated into the MRI-guided cardiac interventions (e.g., transapical valve implantation) to increase its feasibility [153], [154]. In [155], Navkar et al. presented a method to extract the geometric features from MRI images by finding an optimal fit for a circular ring mimicking the valve annulus in the aortic root (see Fig. 26). Moreover, this approach can be used for MRI-guided annuloplasty [150], [152] by dynamically tracking the motion of the annulus.

2) Ventricle segmentation: Cardiac MRI provides important information for diagnosis and treatment of cardiovascular diseases by enabling quantitative assessment of functional parameters of the heart such as ejection fraction, myocardium mass, wall motion, and wall thickness [190]. To measure these functional parameters, many approaches were suggested to identify the main structures of the heart such as the left ventricle (LV) and right ventricle (RV). Fleagle et al. [156] developed a system to delineate the myocardium borders using a minimum-cost path graph search algorithm after the user initialized the center of the LV cavity and the ROI. In [157], Geiger et al. applied dynamic programming to refine the contours indicated by the user to make them correspond to image edges. Goshtasby and Turner [158] proposed a two-

step algorithm combining intensity thresholding to recover the bright blood and local gradient to outline the strong edges using elastic curves. Weng et al. [191] developed an algorithm to threshold the image based on parameters estimated during a learning phase and gain a good approximation of the segmentation.

A number of automatic approaches incorporated prior knowledge of heart shape and motion to improve the segmentation accuracy and robustness. Montagnat and Delingette [162] developed a framework to track the LV motion in 4D noisy or low contrast medical images based on 4D deformable surface models. The proposed method relies on complementary spatial and temporal constraints to regularize the deformation while introducing prior information of the LV shape and motion during the segmentation process. The resulting surface models are well suited for estimating quantitative parameters such as endocardium volume or wall thickness. In [160], Lorenzo-Valdes et al. proposed a method for the segmentation and tracking of the LV, RV and myocardium in 4D cardiac MRI images. Taking advantage of the temporal relation between images, they achieved convincing results by volumetric atlas matching using B-spline registration. However, the efficiency of this approach is low. In [163], Mitchell et al. combined the fast and robust active shape and appearance models [132], [192] in a multistage fashion to extract the LV and RV borders from MRI images. The developed method yielded promising results (see Fig. 27a). However, statistical shape models cannot capture variability outside the training set, which is likely to occur in clinical setting. In addition, appearance modeling may fail in the presence of large gray value variability across subjects and time. The authors in [193] presented a segmentation technique to automatically extract
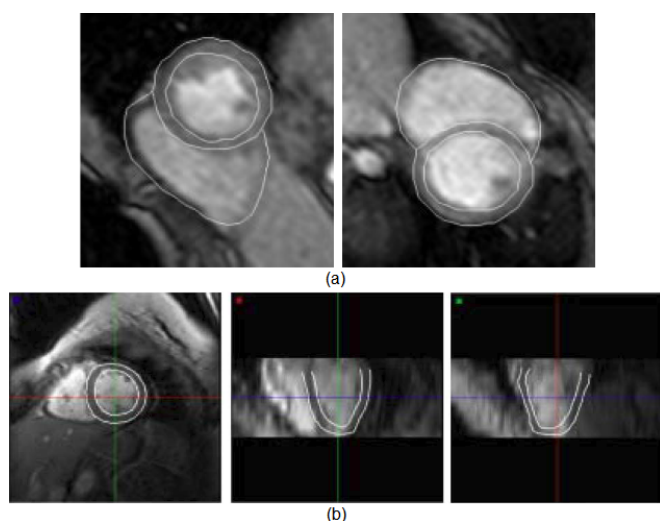
Fig. 27. Segmentation of ventricle borders in cardiac MRI images. (a) LV and RV contours extracted by a multistage hybrid method [163], and (b) LV borders detected by a deformable model in three orthogonal views from the end-diastolic phase [159].

the myocardium in 4D cardiac MR images for quantitative cardiac analysis and the diagnosis of patients. In [159], Kaus et al. proposed to integrate several sources of prior information learned from annotated image data into a deformable model including a deterministic, parametric model of the variation of surface features, inter- and intra-subject shape variation, and spatial relationships of the epicardium and endocardium to handle multiple objects. The presented technique was applied for automatic LV segmentation in 3D cardiac MRI time series. Fig. 27b gives an example. Quantitative validation of 121 data sets in end-diastolic/end-systolic phase demonstrates its high robustness and accuracy.

3) Atrium segmentation: Extracting a patient-specific left atrium (LA) model from intraoperative volumetric data (e.g., C-arm CT images) is important in the preoperative planning for transcatheter LA intervention, and it can provide intraoperative visual guidance as well. However, automatic segmentation of the LA along with the left atrial appendage (LAA) and the pulmonary vein (PV) trunks is a challenge problem, due to the large structural variations in the PV drainage patterns [90] and imaging artifacts. Various approaches have been proposed for the LA segmentation, which can be classified into two categories: model-based [87], [139], [141], [164]–[166] and non-model-based methods [86], [167]. The former methods exploit the prior LA shape information to guide the segmentation, while the latter methods do not involve any prior knowledge of the LA shape. With the prior LA shape constraint, the model-based segmentations can avoid leakage around weak or missing boundaries. However, it may be difficult for them to handle the PV structural variations [139]. On the contrary, the non-model-based approaches [86], [167] address the PV variations well, although they cannot provide the underlying anatomical information such as the left inferior PV. Practically, non-model-based segmentations achieve good results on both CT and MRI data sets.

In order to deal with the structural variations and achieve

robust performance on emerging C-arm CT image data, Zheng et al. proposed an automatic part-based LA segmentation algorithm [141]. Instead of utilizing a holistic mean shape model [139], they employed a multi-part-based model to handle the PV variations, which divide the whole LA into chamber body, appendage and four major PVs. In comparison with the mean shape model [139], each part has a simpler anatomical structure. Therefore, it can be segmented well using a model-based approach, namely marginal space learning [140]. After segmentation, all the six parts are merged into one consolidated mesh, with different anatomical structures represented by distinct colors (see Fig. 28). However, it is still hard to accurately segment the connection region to the LA chamber. To tackle this problem, in [87], Zheng et al. suggested a way to precisely segment the ostia region by enforcing both the image boundary delineation accuracy and mesh smoothness.

4) Vessel centerline extraction: Quantitative coronary angiography (QCA) [168], [173], [194] plays an important role in the analysis of coronary artery disease. An important step in QCA is the estimation of vessel centerline, which has been widely used in computing edge gradients and searching for border positions, deriving video-densitometric profiles, measuring the vessel diameters, calculating the lesion symmetry, and reconstructing the 3D structure of vessel segments or the entire artery.

The earlier approach to determine coronary lumen centerline is commonly based on manual tracing of the entire centerline or identifying several centerline points and producing the continuous centerline by interpolation [171], [195]. The manual centerline identification may result in large vessel orientation errors. On the other hand, the lumen centerline can be calculated as a midline between the left and right coronary borders [168], which can be detected at each cross section separately along the vessel [169] or simultaneously extracted [170]. Given an initial start-of-search point, some coronary lumen centerline detection algorithms are based on vessel tracking by preserving the spatial continuity of vessel position, curvature, diameter, and density [171], [172]. Other approaches utilize active contour models (snakes) [173], which are suitable for analysis of angiographic sequences where the vessel centerline is manually or semi-automatically identified in the first frame and the centerlines in subsequent frames are then tracked by the snakes. In arterial tree extraction, the recursive sequential tracking is generally used for the extraction of the artery network skeleton and the directional resampling of the angiogram is utilized to identify the artery borders based on the extracted skeleton [196]. The accuracy of the skeleton affects the artery border extraction. In [197], Haris et al. proposed a method to detect and label the coronary arterial tree using minimal user supervision in single-view angiograms. Each artery segment was analyzed for skeleton and border extraction using morphological operations and watershed transform. Zhou et al. [174] presented an efficient approach for 3D skeleton and centerline generation based on approximate minimum distance field. This method was later extended to volumetric objects in [175], where the skeletons were interpreted as connected centerlines consisting
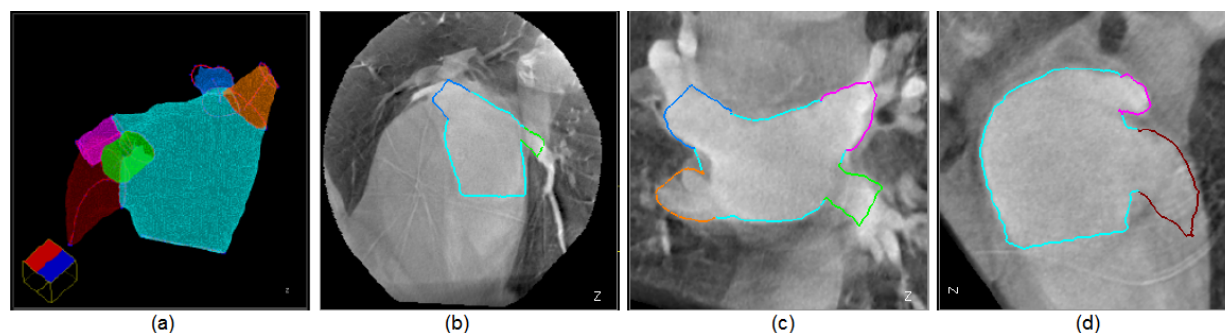
Fig. 28. Extraction of atrium contours in a large CT volume. (a) Part-based LA mesh model (cyan: chamber, red: appendage, green: left inferior PV, magenta: left superior PV, orange: right inferior PV, and blue: right superior PV), and (b-d) LA segmentation results in three orthogonal views with different colors for different mesh parts [141].

of sequences of medial points of consecutive clusters. These centerlines were initially extracted as paths of voxels, followed by medial point replacement, refinement, smoothing and connection operations.

Blondel et al. [198] described a novel method to generate 3D reconstruction of coronary artery centerlines, enabling a 3D tomographic reconstruction of coronary arteries from one single rotational X-ray projection sequence. In [199], Tyrrell et al. employed cylindroidal superellipsoids to model complex tumor microvasculature in 3D imagery, which allows joint estimation of the vessel boundary and centerline, thus approximating the medial axis. The authors in [200] proposed an approach for accurate estimation of vessel centerlines utilizing a ray casting and vote accumulation algorithm (see Fig. 29). Later on, Wong et al. [201] developed an energy-minimization-based framework for the extraction of arterial lumen centerline according to the theory of nonlinear principal curves. They applied a nonparametric model for the representation of lumen centers, and achieved an accuracy of subvoxel level, benefiting the geometric study of aneurysmal neck. The proposed algorithm is adaptive to the vasculature complexity and robust to strongly bended lumen as well as branching vasculature. By registering an elliptical cross-sectional tube with the desired constituent vessel in every major bifurcation of the arterial tree, Wang and Liatsis [202] proposed a deformable tube model-based technique for precise estimation of the centerline and reference lumen surface for both the main vessel and the side branches in the area of bifurcations. Meanwhile, a completely automatic method based on graph-cuts was designed for the accurate extraction of coronary centerline in X-ray angiography imagery [203]. Both methods perform as good as human experts. Motivated by the diffusion tensor image (DTI) field, Cetin et al. [204] proposed an approach using an intensity-based tensor model for the location of coronary artery centerlines from computed tomography angiography (CTA) scans. In [205], a hybrid scheme was reported for the detection of vessel centerlines in preoperative multislice computed tomography (MSCT) sequences, making use of a minimum cost path technique with a fast-marching front propagation. The extracted centerlines are refined in the second procedure by applying an iterative multiscale method based on geometrical moments. Fig. 30 illustrates several vascular centerline extraction results overlaid on the original images in coronary X-ray angiography volumes.

Most of the techniques mentioned above may have difficulty to handle images of poor quality and little work has been done in examining accuracy of the estimated centerline. In most QCA algorithms [173], [194], [213], the validation was based on comparing the extracted centerlines with manually labeled results or generating phantoms with known parameters. The former suffered from a lack of an objective criteria and inter-observer variability, while the latter required a full imaging system to test the software without standard results. Sonka et al. [213] first attempted to evaluate the accuracy of the estimated vessel centerline using indexes that express the position and orientation similarities of two centerlines. In [214], Greenspan et al. described a method to provide an objective accuracy measure for evaluating centerline extraction algorithms. The method compared estimated results with a priori data that was used to generate the centerline. Images of blood vessels with known geometry and centerline were synthesized. They presented a method for an objective comparison of different QCA algorithms and a way for the evaluation of a specific QCA algorithm performance under different geometrical parameters of the vessel. A synthetic vessel-generation tool was applied for the evaluation and comparison of two well-known centerline estimation algorithms. To quantitatively evaluate and compare the performance of existing coronary artery centerline extraction techniques, Schaap et al. [215] presented a standardized evaluation methodology along with a reference database containing 32 cardiac CTA data sets.

IV. COMPARATIVE STUDIES AND DISCUSSIONS

A number of imaging modalities are involved in the minimally invasive transcatheter procedure. Table V shows a summary list of some of these pre-procedural and intra-procedural imaging techniques. The catheter-based imaging techniques like intravascular ultrasound (IVUS) and optical coherence tomography (OCT) are widely used in imaging coronary artery structures, diagnosing and treating coronary diseases such as atherosclerosis [5], [106]. During the whole transcatheter aortic valve implantation (TAVI) procedure [30], [31], various imaging approaches are applied to help place the valve appropriately and minimize the major complications, including multislice computed tomography (MSCT), magnetic resonance imaging (MRI), X-ray angiography/fluoroscopy, and transthoracic/transesophageal echo (TTE/TEE) (refer to Table I for details). To guide the TAVI interventions, MSCT and
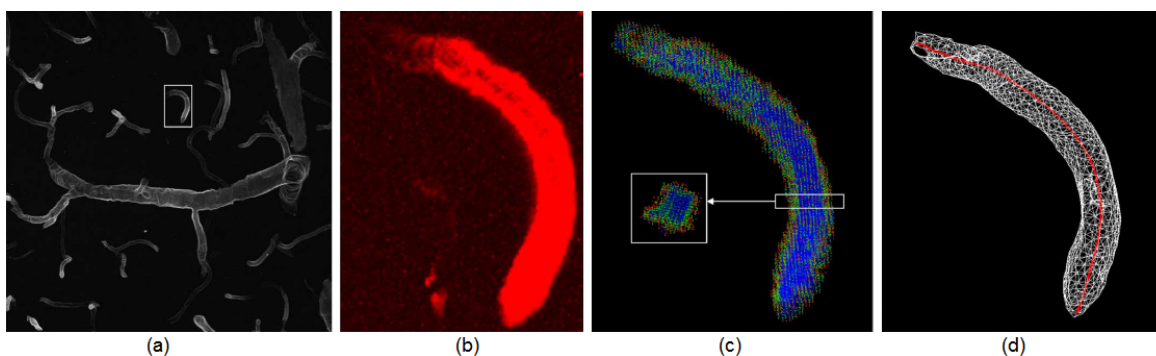
Fig. 29.   Voting-based centerline extraction. (a) Maximum-intensity projection of a confocal data set, (b) enlarged and rendered volume of the selected vessel segment in (a), (c) voting results overlaid on the surface rendering (sliced region shows the cross-section), and (d) detected centerline in red and the surface rendering [200].
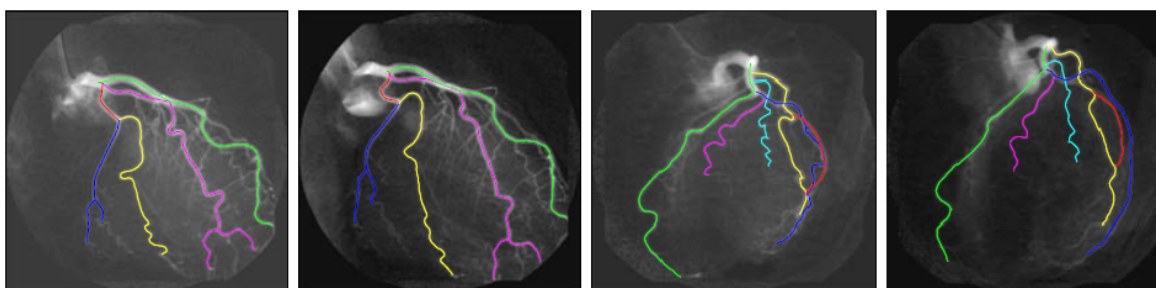

Fig. 30.   Detected centerlines overlaying on original coronary angiography images [206].

TABLE V
IMAGING MODALITIES AND THEIR APPLICATIONS.

Imaging Modality	Applicability
Intravascular ultrasound (IVUS)	Imaging and assessment of coronary arteries and atherosclerosis [5], [106]
Optical coherence tomography (OCT)	Imaging and assessment of coronary arteries and atherosclerosis [5], [106]
Multislice computed tomography (MSCT)	Transcatheter aortic valve implantation [30], [31] Aortic annulus feature evaluation [151] Left atrium segmentation [164]
C-arm computed tomography (C-arm CT)	Left atrium modeling [87], [141], [149]
Computed tomography angiography (CTA)	Left atrium segmentation [86]
Magnetic resonance imaging (MRI)	Transcatheter aortic valve implantation [30], [31] Aortic annulus feature evaluation and motion tracking [42], [150], [155]
Magnetic resonance angiography (MRA)	Left atrium segmentation [86]
X-ray angiography/fluoroscopy	Transcatheter aortic valve implantation [30], [31]
Rotational X-ray angiography (RA)	Intraoperative imaging of left atrium and pulmonary veins to guide catheter ablation of atrial fibrillation [207], [208]
Transthoracic/Transesophageal echo (TTE/TEE)	Transcatheter aortic valve implantation [30], [31] Aortic annulus feature evaluation [151]
Electroanatomical mapping (EAM) + CT/MRI	Imaging cardiac anatomy to guide catheter ablation of atrial fibrillation [209]–[211] and ventricular tachycardia [210], [212]

TTE/TEE are generally employed to preoperatively measure the geometric features (e.g., diameter, center, orientation) of the aortic valve annulus [151]. Moreover, MRI is utilized to evaluate the aortic annulus features and tracking its motion [42], [150], [155], benefiting both preoperative planning and intraoperative guidance for TAVI. It should be noted that there are certain limitations with these imaging technologies. For example, MSCT involves ionizing radiation, TTE provides a limited field of view (FOV), TEE requires access through the esophagus, and MRI offers limited access to the patients inside cylindrical MR scanners.

Interventional cardiac electrophysiology (EP) procedures such as transcatheter left atrial fibrillation ablation require accurate segmentation and labeling of the left atrium (LA) and pulmonary veins (PVs). Computed tomography angiography (CTA), magnetic resonance angiography (MRA), and MSCT can provide preoperative images for this purpose [86], [164]. The integration of preoperative CT or MRI with electroanatomical mapping (EAM) produces more anatomical information of the LA and PVs, which can be used for the guidance of the catheter ablation procedure [209]–[211]. Recently, C-arm computed tomography (C-arm CT) is

TABLE VI
MEASUREMENT OF SEGMENTATION ACCURACY.

Performance Metric	Reference
Jaccard similarity coefficient (Jaccard score)	[219], [220]
Dice similarity coefficient (F-measure)	[221], [222]
Symmetric surface-to-surface distance	[87], [140], [141]
Average surface distance	[219]
Receiver operating characteristic (ROC) curve	[222]–[224]
Hausdorff distance	[126], [129], [219]
Maximum Hausdorff distance	[219]
Mutual information (entropy)	[222]
Average distance	[129]
Chi-square measure	[223]
C-Factor measure	[218]
Kappa statistic	[221], [225]
Root-mean-square error	[116]

emerged as a new 3D imaging technique to provide images for extracting patient-specific LA model [87], [141], [149]. Compared to conventional CT or MRI, it reflects the current state of the patient's heart chamber anatomy.

Performance evaluation of medical image segmentation techniques is of great significance, which addresses the similarity between the segmentation outcome and desired result, the clinical impact of such a similarity, along with the robustness of the segmentation method in the context of variation in patient anatomies and fluctuations in image properties. A variety of evaluation schemes and criteria (e.g., robustness, precision, accuracy and efficiency) have been presented in the literature [216]–[218], taking clinical relevancy and impact into account. In this work, we focus on metrics for the accuracy measurement. Among many other approaches, cross validation [87], [140], [141] is popularly utilized in the assessment of segmentation accuracy, and the results are generally presented in a confusion matrix. A large number of different metrics have been applied to measure the similarity between the segmentation results by an algorithm and the ground truth labeled by an expert. Table VI shows a summary list of these metrics. Most of them are statistical measures as no spatial relations between image pixels/voxels or edges are considered, assuming spatial independence between those elements.

V. CONCLUSIONS

In this paper, we review the computer vision techniques that are widely used in transcatheter intervention for many medical applications. This review gives us some insights into the state-of-the-art imaging technologies, segmentations and user interventions. Even though the research on transcatheter intervention is expanding rapidly, there are still many challenges to be faced. Based on this review, we make the following observations.

1) Compared to traditional open-heart surgery, the minimally invasive transcatheter interventions are less traumatic and offer faster recovery time for patients. In the long term, the transcatheter procedures may encroach upon the conventional surgical approaches.

2) Transcatheter aortic valve implantation (TAVI) emerges as an extremely promising life-saving therapy without requiring a full open-heart surgery. A number of observational clinical studies have demonstrated its feasibility, safety and effectiveness. It will potentially represent the standard of care for patients with severe aortic stenosis. Now it is time to further develop the less traumatic transcatheter valve implantation technology to make it applicable to a wider range of patients.

3) Transcatheter mitral valve repair/replacement (TMVR) is still under development. Innovative solutions properly addressing prosthesis anchoring and sealing in mitral position are highly desirable for clinical applications.

4) With the advent of less invasive and safer transcatheter technologies like TAVI, TMVR, TPVR and TTVI, a new treatment option has become available for patients with inoperable cardiovascular valve stenosis or regurgitation and this treatment may change significantly over the next few years.

5) Percutaneous valve-in-valve implantation has gained increasing acceptance as a feasible treatment option for selected non-surgical patients with degenerated bioprostheses in the aortic, mitral, pulmonary and tricuspid positions. It is also worth noting that manufacturers need to further improve the design of current bioprosthetic valves and more testing is required.

6) While intravascular ultrasound (IVUS) remains the most widely used and validated intravascular imaging technique in clinical practice, optical coherence tomography (OCT) has the potential to become the most accurate imaging modality to assess the lumen dimensions and facilitate the application of automatic measurement algorithms.

7) The good estimation of the guide-wire position is crucial to the elimination of guide-wire shadow artifacts, which will finally benefit the accurate segmentation of the vessel wall in OCT image sequences.

8) Most of current techniques detect the lumen and media-adventitia borders in IVUS images on two distinct data sets. It is desirable to develop algorithms to identify both borders simultaneously.

9) Mid-term and long-term results of a large patient population are highly expected, which will provide useful insights of the transcatheter interventions in the real world. Despite current promising results on transcatheter interventions, there are unsolved issues such as procedural failure and rate of complications. Computer vision techniques could help to minimize these risks and play an important role before, during and after the procedure.

10) Segmentation algorithms could greatly benefit the image-guided transcatheter intervention procedures. There is a clear need of designing efficient and robust segmentation methods with minimal user interaction for the extraction of anatomical structures with higher accuracy during the procedure.

11) Energy minimization-based segmentation approaches like deformable models and graph-cut are very popular in segmenting vessel geometries, providing efficient and

precise knowledge in support of transcatheter procedures.

12) For the extraction of anatomical vessel structures, the integration of prior information (e.g., shape priors) into the segmentation framework could impressively reduce its complexity.

13) The segmentation results allow the construction of anatomical databank, which could possibly be used for exploring the morphological variations, pathological evolution, or growth of organs.

14) These segmentation algorithms are not mutually exclusive. Approaches combining different segmentation techniques are able to produce better results or more anatomical structure information, which is potentially helpful for both preoperative planning and intraoperative guidance during the transcatheter procedures.

15) Machine learning-based segmentation techniques such as marginal space learning are of special interest since the learning algorithms in computer vision are being developed rapidly and promisingly.

16) Performance evaluation in medical image segmentation measures the amount of similarity between the segmented results and the gold standard. Unlike traditional image processing, it needs to consider the clinical aspects including relevancy and impact. Thus, it is fairly important to design or adopt medically-oriented metrics for the measurement of segmentation accuracy, as inappropriate ones may result in serious consequences for transcatheter intervention and consequently the health of patients.

REFERENCES

[1] National Health Service (NHS), UK, http://www.nhs.uk/conditions/cardiovascular-disease/pages/introduction.aspx, Jul. 2012.

[2] University of Maryland Medical Center (UMMC), USA, http://umm.edu/programs/heart/services/programs/surgery/valve-surgery/facts, Mar. 2013.

[3] V. T. Nkomo, J. M. Gardin, and T. N. Skelton, et al., "Burden of valvular heart diseases: a population-based study," *The Lancet*, vol. 368, no. 9540, pp. 1005–1011, Sep. 2006.

[4] http://www.webmd.com/heart-disease/heart-failure/aortic-valve-with-stenosis.

[5] F. Prati and E. Regar, et al., "Expert review document on methodology, terminology, and clinical applications of optical coherence tomography: physical principles, methodology of image acquisition, and clinical application for assessment of coronary arteries and atherosclerosis," *European Heart J.*, vol. 31, no. 4, pp. 401–415, Feb. 2010.

[6] E. Essa, X. Xie, I. Sazonov, P. Nithiarasu, D. Smith, and J. Cotton, "Graph-based segmentation for coronary artery imaging," in *Proc. UK National Conf. Patient-Specific Modelling & Translational Research*, 2013, pp. 1–2.

[7] D. Smith, Cardiology Consultant, Morriston Hospital, Swansea, UK, 2011.

[8] A. Katouzian, E. Angelini, S. G. Carlier, J. S. Suri, N. Navab, and A. F. Laine, "A state-of-the-art review on segmentation algorithms in intravascular ultrasound (IVUS) images," *IEEE Trans. Info. Tech. Biomed.*, vol. 16, no. 5, pp. 823–834, 2012.

[9] M. Sonka, X. Zhang, M. Siebes, M. S. Bissing, S. C. DeJong, S. M. Collins, and C. R. McKay, "Segmentation of intravascular ultrasound images: A knowledge-based approach," *IEEE Trans. Med. Imag.*, vol. 14, no. 4, pp. 719–732, Dec. 1995.

[10] A. Takagi, K. Hibi, X. Zhang, T. J. Teo, H. N. Bonneau, P. G. Yock, and P. J. Fitzgerald, "Automated contour detection for high-frequency intravascular ultrasound imaging: A technique with blood noise reduction for edge enhancement," *Ultrasound Med. Biol.*, vol. 26, no. 6, pp. 1033–1041, Jul. 2000.

[11] E. Essa, X. Xie, I. Sazonov, and P. Nithiarasu, "Automatic IVUS media-adventitia border extraction using double interface graph cut segmentation," in *Proc. IEEE Int. Conf. Image Processing*, 2011, pp. 69–72.

[12] E. Essa, X. Xie, I. Sazonov, P. Nithiarasu, and D. Smith, "Shape prior model for media-adventitia border segmentation in IVUS using graph cut," in *Proc. MICCAI Medical Computer Vision*, 2012, pp. 98–107.

[13] F. Dubuisson, C. Kauffmann, P. Motreff, and L. Sarry, "In vivo OCT coronary imaging augmented with stent reendothelialization score," in *Proc. Int. Conf. Medical Image Computing and Computer Assisted Intervention*, 2009, pp. 475–482.

[14] S. Gurmeric, G. G. Isguder, S. Carlier, and G. Unal, "A new 3-D automated computational method to evaluate in-stent neointimal hyperplasia in in-vivo intravascular optical coherence tomography pullbacks," in *Proc. Med. Image Comput. Comput. Assist. Interv.*, 2009, pp. 776–785.

[15] C. Kauffmann, P. Motreff, and L. Sarry, "In vivo supervised analysis of stent reendothelialization from optical coherence tomography," *IEEE Trans. Med. Imag.*, vol. 29, no. 3, pp. 807–818, 2010.

[16] K. P. Tung, W. Z. Shi, R. D. Silva, E. Edwards, and D. Rueckert, "Automatical vessel wall detection in intravascular coronary OCT," in *Proc. IEEE Int. Symposium Biomedical Imaging: From Nano to Macro*, 2011, pp. 610–613.

[17] P. Généreux, S. J. Head, and D. A. Wood, et al., "Transcatheter aortic valve implantation 10-year anniversary: review of current evidence and clinical implications," *European Heart J.*, vol. 33, no. 19, pp. 2388–2398, Oct. 2012.

[18] F. Zhao and X. Xie, "An overview on interactive medical image segmentation," *Annals of the BMVA*, vol. 2013, no. 7, pp. 1–22, 2013.

[19] http://www.webmd.com/heart/mitral-valve-prolapse-symptoms-causes-and-treatment.

[20] A. Cribier, H. Eltchaninoff, and A. Bash, et al., "Percutaneous transcatheter implantation of an aortic valve prosthesis for calcific aortic stenosis. first human case description," *Circulation*, vol. 106, no. 24, pp. 3006–3008, Dec. 2002.

[21] N. E. Moat, P. Ludman, and M. A. de Belder, et al., "Long-term outcomes after transcatheter aortic valve implantation in high-risk patients with severe aortic stenosis," *J. Am. Coll. Cardiol.*, vol. 58, no. 20, pp. 2130–2138, Nov. 2011.

[22] M. Thomas, G. Schymik, and T. Walther, et al., "Thirty-day results of the SAPIEN aortic bioprosthesis European outcome (SOURCE) registry: A European registry of transcatheter aortic valve implantation using the Edwards SAPIEN valve," *Circulation*, vol. 122, no. 1, pp. 62–69, Jul. 2010.

[23] T. D. Yan, C. Cao, J. Martens-Nielsen, R. Padang, M. Ng, M. P. Vallely, and P. G. Bannon, "Transcatheter aortic valve implantation for high-risk patients with severe aortic stenosis: A systematic review," *J. Thorac. Cardiovasc. Surg.*, vol. 139, no. 6, pp. 1519–1528, Jun. 2010.

[24] H. Eltchaninoff, A. Prat, and M. Gilard, et al., "Transcatheter aortic valve implantation: early results of the FRANCE (FRench Aortic National CoreValve and Edwards) registry," *European Heart J.*, vol. 32, no. 2, pp. 191–197, Jan. 2011.

[25] T. Walther, G. Schuler, M. A. Borger, J. Kempfert, J. Seeburger, Y. Rückert, J. Ender, A. Linke, M. Scholz, V. Falk, and F. W. Mohr, "Transapical aortic valve implantation in 100 consecutive patients: comparison to propensity-matched conventional aortic valve replacement," *European Heart J.*, vol. 31, no. 11, pp. 1398–1403, Jun. 2010.

[26] M. B. Leon and C. R. Smith, et al., "Transcatheter aortic-valve implantation for aortic stenosis in patients who cannot undergo surgery," *New England J. Med.*, vol. 363, no. 17, pp. 1597–1607, Oct. 2010.

[27] http://www.raneyzusman.com/endovascular/transcatheter-aortic-valve-replacement-tavr.html.

[28] S. Bleiziffer, H. Ruge, and J. Hörer, et al., "Predictors for new-onset complete heart block after transcatheter aortic valve implantation," *JACC Cardiovasc. Interv.*, vol. 3, no. 5, pp. 524–530, May 2010.

[29] L. Roten, P. Wenaweser, and E. Delacrétaz, et al., "Incidence and predictors of atrioventricular conduction impairment after transcatheter aortic valve implantation," *American J. Cardiology*, vol. 106, no. 10, pp. 1473–1480, Nov. 2010.

[30] V. Delgado, A. C. Ng, M. Shanks, F. van der Kley, J. D. Schuijf, N. R. van de Veire, L. Kroft, A. de Roos, M. J. Schalij, and J. J. Bax, "Transcatheter aortic valve implantation: role of multimodality cardiac imaging," *Expert Rev. Cardiovasc. Ther.*, vol. 8, no. 1, pp. 113–123, Jan. 2010.

[31] M. Gessat, T. Fraunfelder, L. Altwegg, J. Grünenfelder, and V. Falk, "Transcatheter aortic valve implantation. Role of imaging," *Aswan*

Heart Centre Science & Practice Series, vol. 2011, no. 1, pp. 9–20, Apr. 2011.

[32] Edwards Lifesciences Inc., Irvine, California, USA, http://www.edwards.com/products/transcathetervalve/Pages/THVcategory.aspx.

[33] Medtronic Inc., Minneapolis, Minnesota, USA, http://www.corevalve.com/evolut-r/index.htm.

[34] Jenavalve Technology, Inc., Munich, Germany, http://www.jenavalve.de/index.php?id=116&L=0.

[35] Symetis SA, Ecublens, Switzerland, http://www.symetis.com/products/acurate-ta.

[36] A. Vahanian, O. Alfieri, and N. Al-Attar, et al., "Transcatheter valve implantation for patients with aortic stenosis: a position statement from the European Association of Cardio-Thoracic Surgery (EACTS) and the European Society of Cardiology (ESC), in collaboration with the European Association of Percutaneous Cardiovascular Interventions (EAPCI)," *European Heart J.*, vol. 29, no. 11, pp. 1463–1470, Jun. 2008.

[37] R. Zegdi, V. Ciobotaru, M. Noghin, G. Sleilaty, A. Lafont, C. Latrémouille, A. Deloche, and J. N. Fabiani, "Is it reasonable to treat all calcified stenotic aortic valves with a valved stent? Results from a human anatomic study in adults," *J. Am. Coll. Cardiol.*, vol. 51, no. 5, pp. 579–584, Feb. 2008.

[38] C. J. Schultz, A. Moelker, and N. Piazza, et al., "Three dimensional evaluation of the aortic annulus using multislice computer tomography: are manufacturer's guidelines for sizing for percutaneous aortic valve replacement helpful?" *European Heart J.*, vol. 31, no. 7, pp. 849–856, Apr. 2010.

[39] M. John, R. Liao, Y. Zheng, A. Nöttling, J. Boese, U. Kirschstein, J. Kempfert, and T. Walther, "System to guide transcatheter aortic valve implantations based on interventional C-arm CT imaging," in *Proc. Med. Image Comput. Comput. Assist. Interv.*, 2010, pp. 375–382.

[40] S. Jacobs, M. Gessat, T. Walther, and V. Falk, "Three-dimensional template-based planning for transapical aortic valve implantation," *J. Thorac. Cardiovasc. Surg.*, vol. 141, no. 6, pp. 1541–1543, Jun. 2011.

[41] W. Sun, K. Li, and E. Sirois, "Simulated elliptical bioprosthetic valve deformation: implications for asymmetric transcatheter valve deployment," *J. Biomech.*, vol. 43, no. 16, pp. 375–382, Dec. 2010.

[42] K. A. Horvath, D. Mazilu, M. Guttman, A. Zetts, T. Hunt, and M. Li, "Midterm results of transapical aortic valve replacement via real-time magnetic resonance imaging guidance," *J. Thorac. Cardiovasc. Surg.*, vol. 139, no. 2, pp. 424–430, Feb. 2010.

[43] S. Zanon, "New frontiers in transcatheter heart valve technologies," *Clinica*, pp. 18–20, Dec. 2011.

[44] http://www.abbottvascular.com/us/products/structural-heart/mitraclip.html#about-mitral-regurgitation.

[45] J. H. Karimov, A. L. Massiello, and K. Fukamachi, "Overview of current sutureless and transcatheter mitral valve replacement technology," *Expert Rev. Med. Devices*, vol. 10, no. 1, pp. 73–83, Jan. 2013.

[46] P. T. L. Chiam and C. E. Ruiz, "Percutaneous transcatheter mitral valve repair: a classification of the technology," *JACC Cardiovasc. Interv.*, vol. 4, no. 1, pp. 1–13, Jan. 2011.

[47] Abbott Vascular, Inc., Santa Clara, California, USA, http://www.abbottvascular.com/int/mitraclip.html.

[48] T. Feldman, S. Kar, and M. Rinaldi, et al., "Percutaneous mitral repair with the MitraClip system: safety and midterm durability in the initial EVEREST (endovascular valve edge-to-edge repair study) cohort," *J. Am. Coll. Cardiol.*, vol. 54, no. 8, pp. 686–694, Aug. 2009.

[49] S. Kar, "Percutaneous transcatheter mitral valve repair: adding life to years," *J. Am. Coll. Cardiol.*, vol. 62, no. 12, pp. 1062–1064, Sep. 2013.

[50] O. Alfieri, F. Maisano, M. D. Bonis, P. L. Stefano, L. Torracca, M. Oppizzi, and G. L. Canna, "The double-orifice technique in mitral valve repair: a simple solution for complex problems," *J. Thorac. Cardiovasc. Surg.*, vol. 122, no. 4, pp. 674–681, Oct. 2001.

[51] F. Maisano, O. Franzen, and S. Baldus, et al., "Percutaneous mitral valve interventions in the real world: Early and 1-year results from the ACCESS-EU, a prospective, multicenter, nonrandomized post-approval study of the MitraClip therapy in Europe," *J. Am. Coll. Cardiol.*, vol. 62, no. 12, pp. 1052–1061, Sep. 2013.

[52] http://www.cathlabdigest.com/articles/VEITHSymposium-Percutaneous-Mitral-Valve-Repair-MitraClip.

[53] Micro Interventional Devices, Inc, Langhorne, Pennsylvania, USA, http://www.microinterventional.com/.

[54] CardiAQ Valve Technologies, Inc., Irvine, California, USA, http://www.cardiaq.com/.

[55] H. Ghawi, D. Kenny, and Z. M. Hijazi, "Transcatheter pulmonary valve replacement," *Cardiol. Ther.*, vol. 1, no. 1, pp. 1–14, 2012.

[56] P. Bonhoeffer, Y. Boudjemline, Z. Saliba, J. Merckx, Y. Aggoun, D. Bonnet, P. Acar, J. L. Bidois, D. Sidi, and J. Kachaner, "Percutaneous replacement of pulmonary valve in a right-ventricle to pulmonary-artery prosthetic conduit with valve dysfunction," *Lancet*, vol. 356, no. 9239, pp. 1403–1405, Oct. 2000.

[57] P. Bonhoeffer, Y. Boudjemline, S. A. Qureshi, J. L. Bidois, L. Iserin, P. Acar, J. Merckx, J. Kachaner, and D. Sidi, "Percutaneous insertion of the pulmonary valve," *J. Am. Coll. Cardiol.*, vol. 39, no. 10, pp. 1664–1669, May 2002.

[58] S. Khambadkone, L. Coats, and A. Taylor, et al., "Percutaneous pulmonary valve implantation in humans: results in 59 consecutive patients," *Circulation*, vol. 112, no. 8, pp. 1189–1197, Aug. 2005.

[59] F. Garay, J. Webb, and Z. M. Hijazi, "Percutaneous replacement of pulmonary valve using the Edwards-Cribier percutaneous heart valve: first report in a human patient," *Catheter. Cardiovasc. Interv.*, vol. 67, no. 5, pp. 659–662, May 2006.

[60] P. Lurz, L. Coats, and S. Khambadkone, et al., "Percutaneous pulmonary valve implantation: impact of evolving technology and learning curve on clinical outcome," *Circulation*, vol. 117, no. 15, pp. 1964–1972, Apr. 2008.

[61] D. B. McElhinney, W. E. Hellenbrand, E. M. Zahn, T. K. Jones, J. P. Cheatham, J. E. Lock, and J. A. Vincent, "Short- and medium-term outcomes after transcatheter pulmonary valve placement in the expanded multicenter US melody valve trial," *Circulation*, vol. 122, no. 5, pp. 507–516, Aug. 2010.

[62] D. Kenny, Z. M. Hijazi, S. Kar, J. Rhodes, M. Mullen, R. Makkar, G. Shirali, M. Fogel, J. Fahey, M. G. Heitschmidt, and C. Cain, "Percutaneous implantation of the Edwards SAPIEN transcatheter heart valve for conduit failure in the pulmonary position: early phase 1 results from an international multicenter clinical trial," *J. Am. Coll. Cardiol.*, vol. 58, no. 21, pp. 2248–2256, Nov. 2011.

[63] http://newsroom.medtronic.com/phoenix.zhtml?c=251324&p=irol-mediakit&ID=MelodyTranscatheterPulmonaryValve.

[64] J. Nordmeyer, S. Khambadkone, L. Coats, S. Schievano, P. Lurz, G. Parenzan, A. M. Taylor, J. E. Lock, and P. Bonhoeffer, "Risk stratification, systematic classification, and anticipatory management strategies for stent fracture after percutaneous pulmonary valve implantation," *Circulation*, vol. 115, no. 11, pp. 1392–1397, Mar. 2007.

[65] S. Schievano, L. Petrini, F. Migliavacca, L. Coats, J. Nordmeyer, P. Lurz, S. Khambadkone, A. M. Taylor, G. Dubini, and P. Bonhoeffer, "Finite element analysis of stent deployment: understanding stent fracture in percutaneous pulmonary valve implantation," *J. Interv. Cardiol.*, vol. 20, no. 6, pp. 546–554, Dec. 2007.

[66] D. B. McElhinney, J. P. Cheatham, T. K. Jones, J. E. Lock, J. A. Vincent, E. M. Zahn, and W. E. Hellenbrand, "Stent fracture, valve dysfunction, and right ventricular outflow tract reintervention after transcatheter pulmonary valve implantation: patient-related and procedural risk factors in the US Melody valve trial," *Circ. Cardiovasc. Interv.*, vol. 4, no. 6, pp. 602–614, Dec 2011.

[67] S. P. Batlivala, S. Emani, J. E. Mayer, and D. B. McElhinney, "Pulmonary valve replacement function in adolescents: a comparison of bioprosthetic valves and homograft conduits," *Ann. Thorac. Surg.*, vol. 93, no. 6, pp. 2007–2016, Jun. 2012.

[68] J. Nordmeyer, L. Coats, P. Lurz, T. Y. Lee, G. Derrick, P. Rees, S. Cullen, A. M. Taylor, S. Khambadkone, and P. Bonhoeffer, "Percutaneous pulmonary valve-in-valve implantation: a successful treatment concept for early device failure," *European Heart J.*, vol. 29, no. 6, pp. 810–815, Mar. 2008.

[69] H. Weich, "Transcatheter tricuspid valve replacement," *Interv. Cardiol.*, vol. 7, no. 1, pp. 59–62, 2012.

[70] M. Gewillig and C. Dubois, "Percutaneous re-revalvulation of the tricuspid valve," *Catheter Cardiovasc. Interv.*, vol. 77, no. 5, pp. 692–695, Apr. 2011.

[71] P. A. Calvert, D. Himbert, E. Brochet, C. Radu, B. Iung, U. Hvass, J. M. Darondel, J. P. Depoix, P. Nataf, and A. Vahanian, "Transfemoral implantation of an Edwards SAPIEN valve in a tricuspid bioprosthesis without fluoroscopic landmarks," *EuroInterv.*, vol. 7, no. 11, pp. 1336–1339, Mar. 2012.

[72] E. S. Hoendermis, Y. L. Douglas, and A. F. van den Heuvel, "Percutaneous Edwards SAPIEN valve implantation in the tricuspid position: case report and review of literature," *EuroInterv.*, vol. 8, no. 5, pp. 628–633, Sep. 2012.

[73] M. Greif, R. Schramm, G. Steinbeck, C. Hagl, C. Schmitz, and C. Kupatt, "Transfemoral access for valve in valve implantation of an Edwards Sapien XT valve in a stenotic tricuspid bioprosthesis under fluoroscopic guidance," *Canadian J. Cardiology*, vol. 29, no. 8, pp. 1014.e3–e4, Aug. 2013.

[74] B. Daneault, M. R. Williams, M. B. Leon, J. M. Paradis, and S. K. Kodali, "Transcatheter tricuspid valve-in-valve replacement resulting in 4 different prosthetic heart valves in a single patient," *J. Am. Coll. Cardiol.*, vol. 61, no. 2, p. e3, Jan. 2013.

[75] F. Ribichini, G. Pesarini, M. Feola, M. Agostini, G. Molinari, A. Rossi, G. Faggian, and C. Vassanelli, "Transcatheter tricuspid valve implantation by femoral approach in trivalvular heart disease," *American J. Cardiology*, vol. 112, no. 7, pp. 1051–1053, Oct. 2013.

[76] A. Lauten, M. Ferrari, K. Hekmat, R. Pfeifer, G. Dannberg, A. Ragoschke-Schumm, and H. R. Figulla, "Heterotopic transcatheter tricuspid valve implantation: first-in-man application of a novel approach to tricuspid regurgitation," *European Heart J.*, vol. 32, no. 10, pp. 1207–1213, May 2011.

[77] P. A. Roberts, Y. Boudjemline, and J. P. Cheatham, et al., "Percutaneous tricuspid valve replacement in congenital and acquired heart disease," *J. Am. Coll. Cardiol.*, vol. 58, no. 2, pp. 117–122, Jul. 2011.

[78] http://mykentuckyheart.com/information/TricuspidRegurgitation.htm.

[79] J. Therrien, S. C. Siu, P. R. McLaughlin, P. P. Liu, W. G. Williams, and G. D. Webb, "Pulmonary valve replacement in adults late after repair of tetralogy of fallot: are we operating too late?" *J. Am. Coll. Cardiol.*, vol. 36, no. 5, pp. 1670–1675, Nov. 2000.

[80] J. G. Webb, D. A. Wood, and J. Ye, et al., "Transcatheter valve-in-valve implantation for failed bioprosthetic heart valves," *Circulation*, vol. 121, no. 16, pp. 1848–1857, Apr. 2010.

[81] P. Wenaweser, L. Buellesfeld, U. Gerckens, and E. Grube, "Percutaneous aortic valve replacement for severe aortic regurgitation in degenerated bioprosthesis: the first valve in valve procedure using the Corevalve revalving system," *Catheter. Cardiovasc. Interv.*, vol. 70, no. 5, pp. 760–764, Nov. 2007.

[82] L. A. F. M. van Garsse, R. M. A. ter Bekke, and V. G. V. A. van Ommen, "Percutaneous transcatheter valve-in-valve implantation in stenosed tricuspid valve bioprosthesis," *Circulation*, vol. 123, no. 5, pp. e219–221, Feb. 2011.

[83] H. Weich, J. Janson, J. van Wyk, P. Herbst, P. le Roux, and A. Doubell, "Transjugular tricuspid valve-in-valve replacement," *Circulation*, vol. 124, no. 5, pp. e157–160, Aug. 2011.

[84] C. Jux, H. Akintuerk, and D. Schranz, "Two melodies in concert: transcatheter double-valve replacement," *Catheter. Cardiovasc. Interv.*, vol. 80, no. 6, pp. 997–1001, Nov. 2012.

[85] A. Lauten, H. R. Figulla, C. Willich, A. Laube, W. Rademacher, H. Schubert, S. Bischoff, and M. Ferrari, "Percutaneous caval stent valve implantation: investigation of an interventional approach for treatment of tricuspid regurgitation," *European Heart J.*, vol. 31, no. 10, pp. 1274–1281, May 2010.

[86] M. John and N. Rahn, "Automatic left atrium segmentation by cutting the blood pool at narrowings," in *Proc. Med. Image Comput. Comput. Assist. Interv.*, 2005, pp. 798–805.

[87] Y. Zheng, M. John, J. Boese, and D. Comaniciu, "Precise segmentation of the left atrium in C-arm CT volumes with applications to atrial fibrillation ablation," in *Proc. IEEE Int. Sym. Biomedical Imaging*, 2012, pp. 1421–1424.

[88] C. Pappone, S. Rosanio, and G. Oreto, et al., "Circumferential radiofrequency ablation of pulmonary vein ostia: A new anatomic approach for curing atrial fibrillation," *Circulation*, vol. 102, no. 21, pp. 2619–2628, Nov. 2000.

[89] H. Oral, C. Pappone, and A. Chugh, et al., "Circumferential pulmonary-vein ablation for chronic atrial fibrillation," *New England J. Med.*, vol. 354, no. 9, pp. 934–941, Mar. 2006.

[90] E. M. Marom, J. E. Herndon, Y. H. Kim, and H. P. McAdams, "Variations in pulmonary venous drainage to the left atrium: implications for radiofrequency ablation," *Radiology*, vol. 230, no. 3, pp. 824–829, Mar. 2004.

[91] C. C. Lang, V. Santinelli, and G. Augello, et al., "Transcatheter radiofrequency ablation of atrial fibrillation in patients with mitral valve prostheses and enlarged atria: safety, feasibility, and efficacy," *J. Am. Coll. Cardiol.*, vol. 45, no. 6, pp. 868–872, Mar. 2005.

[92] C. Pappone, G. Oreto, and S. Rosanio, et al., "Atrial electroanatomic remodeling after circumferential radiofrequency pulmonary vein ablation: efficacy of an anatomic approach in a large cohort of patients with atrial fibrillation," *Circulation*, vol. 104, no. 21, pp. 2539–2544, Nov. 2001.

[93] C. Pappone, S. Rosanio, and G. Augello, et al., "Mortality, morbidity, and quality of life after circumferential pulmonary vein ablation for atrial fibrillation: outcomes from a controlled nonrandomized long-term study," *J. Am. Coll. Cardiol.*, vol. 42, no. 2, pp. 185–197, Jul. 2003.

[94] C. E. Mesas, C. Pappone, and C. C. Lang, et al., "Left atrial tachycardia after circumferential pulmonary vein ablation for atrial fibrillation:

[95] M. R. Karch, B. Zrenner, and I. Deisenhofer, et al., "Freedom from atrial tachyarrhythmias after catheter ablation of atrial fibrillation: a randomized comparison between 2 current ablation strategies," *Circulation*, vol. 111, no. 22, pp. 2875–2880, Jun. 2005.

[96] http://www.heart-valve-surgery.com/heart-surgery-blog/2012/02/22/sapien-redo-operations-eric-roselli-dr/.

[97] http://healthyhabitshotline.com/atrial-fibrillation-a-fib.

[98] http://www.thewellingtoncardiacservices.com/our-treatments-cardiology.asp.

[99] S. Manganiello, M. Anselmino, and C. Amellone, et al., "Symptomatic and asymptomatic long-term recurrences following transcatheter atrial fibrillation ablation," *Pacing Clin. Electrophysiol.*, vol. 37, no. 6, pp. 697–702, Jun. 2014.

[100] C. Pappone, H. Oral, and V. Santinelli, et al., "Atrio-esophageal fistula as a complication of percutaneous transcatheter ablation of atrial fibrillation," *Circulation*, vol. 109, no. 22, pp. 2724–2726, Jun. 2004.

[101] C. E. Moss, S. Fernandez-Caballero, and D. Walker, "Atrio-oesophageal fistula after transcatheter radiofrequency ablation," *BMJ Case Rep.*, Jan. 2015.

[102] E. Essa, "Combinatorial optimisation for arterial image segmentation," Ph.D. dissertation, Swansea University, 2014.

[103] C. D. Mario, G. Görge, R. Peters, P. Kearney, F. Pinto, D. Hausmann, C. von Birgelen, A. Colombo, H. Mudra, J. Roelandt, and R. Erbel, "Clinical application and image interpretation in intracoronary ultrasound," *European Heart J.*, vol. 19, no. 2, pp. 207–229, Feb. 1998.

[104] G. S. Mintz, S. E. Nissen, and W. D. Anderson, et al., "ACC Clinical expert consensus document on standards for acquisition, measurement and reporting of intravascular ultrasound studies (IVUS)," *J. Am. Coll. Cardiol.*, vol. 37, no. 5, pp. 1478–1492, Apr. 2001.

[105] D. Huang, E. A. Swanson, C. P. Lin, J. S. Schuman, W. G. Stinson, W. Chang, M. R. Hee, T. Flotte, K. Gregory, and C. A. Puliafito, "Optical coherence tomography," *Science*, vol. 254, pp. 1178–1181, 1991.

[106] Y. Kawase, K. Hoshino, R. Yoneyama, J. McGregor, R. J. Hajjar, I. K. Jang, and M. Hayase, "In vivo volumetric analysis of coronary stent using optical coherence tomography with a novel balloon occlusion-flushing catheter: a comparison with intravascular ultrasound," *Ultrasound Med. Biol.*, vol. 31, no. 10, pp. 1343–1349, Oct. 2005.

[107] J. G. Fujimoto and J. M. Schmitt, "Principles of OCT," in *Handbook of Optical Coherence Tomography in Cardiovascular Research*, T. G. van Leeuwen and P. Serruys, Eds. Abingdon, UK: Taylor & Francis, 2006, pp. 19–33.

[108] A. Giannopoulos, Y. S. Chatzizisis, and G. D. Giannoglou, "Optical coherence tomography: an arrow in our quiver," *Expert. Rev. Cardiovasc. Ther.*, vol. 10, no. 5, pp. 539–541, May 2012.

[109] J. J. Wentzel, Y. S. Chatzizisis, F. J. H. Gijsen, G. D. Giannoglou, C. L. Feldman, and P. H. Stone, "Endothelial shear stress in the evolution of coronary atherosclerotic plaque and vascular remodelling: current understanding and remaining questions," *Cardiovasc. Res.*, vol. 96, no. 2, pp. 234–243, Nov. 2012.

[110] Y. S. Chatzizisis, V. G. Koutkias, and K. Toutouzas, et al., "Clinical validation of an algorithm for rapid and accurate automated segmentation of intracoronary optical coherence tomography images," *Int. J. Cardiology*, vol. 172, no. 3, pp. 568–580, Apr. 2014.

[111] E. Regar, F. Prati, and P. W. Serruys, "Intracoronary OCT application: methodological considerations," in *Handbook of Optical Coherence Tomography in Cardiovascular Research*, T. G. van Leeuwen and P. Serruys, Eds. Abingdon, UK: Taylor & Francis, 2006, pp. 53–64.

[112] J. Tanigawa, P. Barlis, and C. D. Mario, "Intravascular optical coherence tomography: optimisation of image acquisition and quantitative assessment of stent strut apposition," *EuroInterv.*, vol. 3, pp. 128–136, 2007.

[113] F. Prati, M. Cera, V. Ramazzotti, F. Imola, R. Giudice, and M. Albertucci, "Safety and feasibility of a new non-occlusive technique for facilitated intracoronary optical coherence tomography (OCT) acquisition in various clinical and anatomical scenarios," *EuroInterv.*, vol. 3, pp. 365–370, 2007.

[114] F. Prati, M. Cera, V. Ramazzotti, F. Imola, R. Giudice, M. Giudice, S. D. Propris, and M. Albertucci, "From bench to bedside: A novel technique of acquiring OCT images," *Circulation J.*, vol. 72, no. 5, pp. 839–843, May 2008.

[115] T. Yamaguvhi, M. Terashima, and T. Akasaka, et al., "Safety and feasibility of an intravascular optical coherence tomography image wire

system in the clinical setting," *American J. Cardiology*, vol. 101, no. 5, pp. 562–567, Mar. 2008.

[116] R. W. Downe, A. Wahle, T. Kovarnik, H. Skalicka, J. J. Lopez, J. Horak, and M. Sonka, "Segmentation of intravascular ultrasound images using graph search and a novel cost function," in *Proc. MICCAI Workshop Computer Vision for Intravascular and Intracardiac Imaging*, 2008, pp. 71–79.

[117] D. Meier, R. Cothren, D. Vince, and J. Cornhill, "Automated morphometry of coronary arteries with digital image analysis of intravascular ultrasound," *Amer. Heart J.*, vol. 133, no. 6, pp. 681–690, Jun. 1997.

[118] Z. Luo, Y. Wang, and W. Wang, "Estimating coronary artery lumenarea with optimization-based contour detection," *IEEE Trans. Med. Imag.*, vol. 22, no. 4, pp. 564–566, Apr. 2003.

[119] G. Unal, S. Bucher, S. Carlier, G. Slabaugh, T. Fang, and K. Tanaka, "Shape-driven segmentation of the arterial wall in intravascular ultrasound images," *IEEE Trans. Info. Tech. Biomed.*, vol. 12, no. 3, pp. 335–347, May 2008.

[120] D. Gil, P. Radeva, J. Saludes, and J. Mauri, "Automatic segmentation of artery wall in coronary IVUS images: a probabilistic approach," in *Proc. Computers in Cardiology*, 2000, pp. 687–690.

[121] D. Gil, P. Radeva, and J. Saludes, "Segmentation of artery wall in coronary IVUS images: A probabilistic approach," in *Proc. Int. Conf. Pattern Recog.*, 2000, pp. 352–355.

[122] E. Mendizabal-Ruiz, M. Rivera, and I. A. Kakadiaris, "A probabilistic segmentation method for the identification of luminal borders in intravascular ultrasound images," in *Proc. IEEE Conf. Comput. Vis. Pattern Recog.*, 2008, pp. 1–8.

[123] A. Taki, Z. Najafi, A. Roodaki, S. K. Setarehdan, R. A. Zoroofi, A. Konig, and N. Navab, "Automatic segmentation of calcified plaques and vessel borders in IVUS images," *Int. J. CARS*, vol. 3, pp. 347–354, 2008.

[124] C. Haas, H. Ermert, S. Holt, P. Grewe, A. Machraoui, and J. Barmeyer, "Segmentation of 3D intravascular ultrasonic images based on a random field model," *Ultrasound Med. Biol.*, vol. 26, no. 2, pp. 297–306, Feb. 2000.

[125] E. Brusseau, C. L. de Korte, F. Mastik, J. Schaar, and A. F. W. van der Steen, "Fully automatic luminal contour segmentation in intracoronary ultrasound imaging - a statistical approach," *IEEE Trans. Med. Imag.*, vol. 23, no. 5, pp. 554–566, May 2004.

[126] M. R. Cardinal, J. Meunier, G. Soulez, R. L. Maurice, E. Therasse, , and G. Cloutier, "Intravascular ultrasound image segmentation: A three-dimensional fast-marching method based on gray level distribution," *IEEE Trans. Med. Imag.*, vol. 25, no. 5, pp. 590–601, May 2006.

[127] M. Kass, A. Witkin, and D. Terzopoulos, "Snakes: Active contour models," *Int. J. Comput. Vis.*, vol. 1, no. 4, pp. 321–331, 1988.

[128] H. Eviatar and R. L. Somorjai, "A fast simple active contour algorithm for biomedical images," *Pattern Recognition Letters*, vol. 17, pp. 969–974, 1996.

[129] R. Shekhar, R. M. Cothren, D. G. Vince, S. Chandra, J. D. Thomas, and J. F. Cornhill, "Three-dimensional segmentation of luminal and adventitial borders is serial intravascular ultrasound images," *Computer. Med. Imag. Graphics*, vol. 23, no. 6, pp. 299–309, 1999.

[130] G. Kovalski, R. Beyar, R. Shofti, and H. Azhari, "Three-dimensional automatic quantitative analysis of intravascular ultrasound images," *Ultrasound Med. Biol.*, vol. 26, no. 4, pp. 527–537, May 2000.

[131] T. F. Cootes, A. Hill, C. J. Taylor, and J. Graham, "The use of active shape models for locating structures in medical images," *Imag. Vis. Comp.*, vol. 12, no. 6, pp. 355–366, Jul. 1994.

[132] T. F. Cootes, C. J. Taylor, D. H. Cooper, and J. Graham, "Active shape models - their training and application," *Comp. Vis. Imag. Under.*, vol. 61, no. 1, pp. 38–59, Jan. 1995.

[133] A. Kelemen, G. Szekely, and G. Gerig, "Elastic model-based segmentation of 3-D neuroradiological data sets," *IEEE Trans. Med. Imag.*, vol. 18, no. 10, pp. 828–839, 1999.

[134] T. McInerney and D. Terzopoulos, "Deformable models in medical image analysis: A survey," *Med. Imag. Anal.*, vol. 1, no. 2, pp. 91–108, 1996.

[135] L. H. Staib and J. S. Duncan, "Model-based deformable surface finding for medical images," *IEEE Trans. Med. Imag.*, vol. 15, no. 5, pp. 720–731, 1996.

[136] J. Weese, M. Kaus, C. Lorenz, S. Lobregt, R. Truyen, and V. Pekar, "Shape constrained deformable models for 3D medical image segmentation," in *Information Processing in Medical Imaging*, vol. 2082. New York: Springer, 2001, pp. 380–387.

[137] O. Ecabert, J. Peters, H. Schramm, C. Lorenz, J. von Berg, M. Walker, M. Vembar, M. Olszewski, K. Subramanyan, and G. L. J. Weese,

[138] "Automatic model-based segmentation of the heart in CT images," *IEEE Trans. Med. Imag.*, vol. 27, no. 9, pp. 1189–1201, Sep. 2008.

[138] J. Peters, O. Ecabert, C. Lorenz, J. von Berg, M. Walker, M. Vembar, M. Olszewski, and J.Weese, "Segmentation of the heart and major vascular structures in cardiovascular CT images," in *Proc. SPIE Conf. Medical Imaging*, 2008, pp. 691 417–1–12.

[139] R. Manzke, C. Meyer, O. Ecabert, J. Peters, N. J. Noordhoek, A. Thiagalingam, V. Y. Reddy, R. C. Chan, and J. Weese, "Automatic segmentation of rotational X-ray images for anatomic intra-procedural surface generation in atrial fibrillation ablation procedures," *IEEE Trans. Medical Imaging*, vol. 29, no. 2, pp. 260–272, 2010.

[140] Y. Zheng, A. Barbu, B. Georgescu, M. Scheuering, and D. Comaniciu, "Four-chamber heart modeling and automatic segmentation for 3-D cardiac CT volumes using marginal space learning and steerable features," *IEEE Trans. Medical Imaging*, vol. 27, no. 11, pp. 1668–1681, 2008.

[141] Y. Zheng, T. Wang, M. John, S. K. Zhou, J. Boese, and D. Comaniciu, "Multi-part left atrium modeling and segmentation in C-arm CT volumes for atrial fibrillation ablation," in *Proc. Med. Image Comput. Comput. Assist. Interv.*, 2011, pp. 487–495.

[142] A. Wahle, J. J. Lopez, M. E. Olszewski, S. C. Vigmostad, K. B. Chandran, J. D. Rossen, and M. Sonka, "Plaque development, vessel curvature, and wall shear stress in coronary arteries assessed by x-ray angiography and intravascular ultrasound," *Med. Imag. Anal.*, vol. 10, no. 4, pp. 615–631, 2006.

[143] K. Li, X. Wu, D. Z. Chen, and M. Sonka, "Optimal surface segmentation in volumetric images - a graph-theoretic approach," *IEEE Trans. Pattern Anal. Mach. Intell.*, vol. 28, no. 1, pp. 119–134, 2006.

[144] A. Katouzian, B. Baseri, E. E. Konofagou, and A. F. Laine, "Automatic detection of blood versus non-blood regions on intravascular ultrasound (IVUS) images using wavelet packet signatures," in *Proc. SPIE Conf. Medical Imaging*, 2008, pp. 69 200H1–8.

[145] M. Papadogiorgaki, V. Mezaris, Y. Chatzizisis, G. Giannoglou, and I. Kompatsiaris, "Image analysis techniques for automated IVUS contour detection," *Ultrasound Med. Biol.*, vol. 34, no. 9, pp. 1482–1498, Sep. 2008.

[146] A. Katouzian, E. D. Angelini, A. Lorsakul, B. Sturm, and A. F. Laine, "Lumen border detection of intravascular ultrasound via denoising of directional wavelet representations," in *Proc. Functional Imaging and Modeling of the Heart*, 2009, pp. 104–113.

[147] A. Katouzian, E. D. Angelini, B. Sturm, and A. F. Laine, "Automatic detection of luminal borders in IVUS images by magnitude-phase histograms of complex brushlet coefficients," in *Proc. IEEE Eng. Med. Biol. Soc.*, 2010, pp. 3073–3076.

[148] D. Gil, A. Hernandez, O. Rodriguez, J. Mauri, and P. Radeva, "Statistical strategy for anisotropic adventitia modeling in IVUS," *IEEE Trans. Med. Imag.*, vol. 25, no. 6, pp. 768–778, Jun. 2006.

[149] D. Yang, Y. Zheng, and M. John, "Graph cuts based left atrium segmentation refinement and right middle pulmonary vein extraction in C-arm CT," in *Proc. SPIE Conf. Medical Imaging*, 2013, pp. 1–9.

[150] E. R. McVeigh, M. A. Guttman, R. J. Lederman, M. Li, O. Kocaturk, T. Hunt, S. Kozlov, and K. A. Horvath, "Real-time interactive MRI-guided cardiac surgery: Aortic valve replacement using a direct apical approach," *Magn. Reson. Med.*, vol. 56, no. 5, pp. 958–964, Nov. 2006.

[151] A. Hutter, A. Opitz, S. Bleiziffer, H. Ruge, I. Hettich, D. Mazzitelli, A. Will, R. Tassani, R. Bauernschmitt, and R. Lange, "Aortic annulus evaluation in transcatheter aortic valve implantation," *Catheter. Cardiovasc. Interv.*, vol. 76, no. 7, pp. 1009–1019, Dec. 2010.

[152] M. Li, D. Mazilu, and K. A. Horvath, "Robotic system for transapical aortic valve replacement with MRI guidance," in *Proc. Med. Image Comput. Comput. Assist. Interv.*, 2008, pp. 476–484.

[153] M. Li, A. Kapoor, D. Mazilu, B. Wood, and K. A. Horvath, "Cardiac interventions under MRI guidance using robotic assistance," in *Proc. IEEE Int. Conf. Robotics and Automation*, May 2010, pp. 2574–2579.

[154] E. Yeniaras, J. Lamaury, Z. Deng, and N. V. Tsekos, "Towards a new cyber-physical system for MRI-guided and robot-assisted cardiac procedures," in *Proc. IEEE Int. Conf. Information Technology and Applications in Biomedicine*, Nov. 2010, pp. 1–5.

[155] N. V. Navkar, E. Yeniaras, D. J. Shah, N. V. Tsekos, and Z. Deng, "Extracting geometric features of aortic valve annulus motion from dynamic MRI for guiding interventions," in *Proc. IEEE Int. Sym. Biomedical Imaging: From Nano to Macro*, 2011, pp. 1302–1305.

[156] S. R. Fleagle, D. R. Thedens, J. C. Ehrhardt, T. D. Scholz, and D. J. Skorton, "Automated identification of left ventricular borders from spin-echo magnetic resonance images," *Invest. Radiol.*, vol. 26, no. 4, pp. 295–303, Apr. 1991.

[157] D. Geiger, A. Gupta, L. A. Costa, and J. Vlontzos, "Dynamic programming for detecting, tracking, and matching deformable contours," *IEEE Trans. Pattern Anal. Mach. Intell.*, vol. 17, no. 3, pp. 294–302, 1995.

[158] A. Goshtasby and D. A. Turner, "Segmentation of cardiac cine MR images for extraction of right and left ventricular chambers," *IEEE Trans. Med. Imag.*, vol. 14, no. 1, pp. 56–64, Mar. 1995.

[159] M. R. Kaus, J. von Berg, J. Weese, W. Niessen, and V. Pekar, "Automated segmentation of the left ventricle in cardiac MRI," *Med. Imag. Anal.*, vol. 8, no. 3, pp. 245–254, Sep. 2004.

[160] M. Lorenzo-Valdés, G. Sanchez-Ortiz, R. Mohiaddin, and D. Rueckert, "Atlas-based segmentation and tracking of 3D cardiac MR images using non-rigid registration," in *Proc. Med. Image Comput. Comput. Assist. Interv.*, 2002, pp. 642–650.

[161] T. F. Cootes and C. J. Taylor, "Statistical models of appearance for medical image analysis and computer vision," in *Proc. SPIE Conf. Medical Imaging*, 2001, pp. 236–248.

[162] J. Montagnat and H. Delingette, "Space and time shape constrained deformable surfaces for 4D medical image segmentation," in *Proc. Med. Image Comput. Comput. Assist. Interv.*, 2000, pp. 196–205.

[163] S. C. Mitchell, B. P. F. Lelieveldt, R. J. van der Geest, H. G. Bosch, J. H. C. Reiber, and M. Sonka, "Multistage hybrid active appearance model matching: segmentation of left and right ventricles in cardiac MR images," *IEEE Trans. Med. Imag.*, vol. 20, no. 5, pp. 415–423, May 2001.

[164] J. von Berg and C. Lorenz, "Accurate left atrium segmentation in multislice CT images using a shape model," in *Proc. SPIE Conf. Medical Imaging*, 2005, pp. 351–360.

[165] R. Karim, C. Juli, L. M. Lawes, P. Kanangaratnam, D. W. Davies, N. S. Peters, and D. Rueckert, "Automatic segmentation of left atrial geometry from contrast-enhanced magnetic resonance images using a probabilistic atlas," in *Proc. MICCAI Workshop STACOM*, 2010, pp. 134–143.

[166] M. Depa, M. R. Sabuncu, G. Holmvang, R. Nezafat, E. J. Schmidt, and P. Golland, "Robust atlas-based segmentation of highly variable anatomy: Left atrium segmentation," in *Proc. MICCAI Workshop STACOM*, 2010, pp. 85–94.

[167] R. Karim, R. Mohiaddin, and D. Rueckert, "Left atrium segmentation for atrial fibrillation ablation," in *Proc. SPIE Conf. Medical Imaging: Visualization, Image-guided Procedures, and Modeling*, 2008, p. 69182U.

[168] J. H. C. Reiber, P. W. Serruys, and J. D. Barth, "Quantitative coronary angiography," in *Cardiac Imaging, M. L. Marcus, H. R. Schelbert, D. J. Skorton and G. L. Wolf, Eds., Philadelphia, PA: Saunders*, 1991, pp. 211–280.

[169] T. N. Pappas and J. S. Lim, "A new method for estimation of coronary artery dimensions in angiograms," *IEEE Trans. Acoust., Speech, Signal Processing*, vol. 36, no. 9, pp. 1501–1513, Sep. 1988.

[170] M. Sonka, M. D. Winniford, and S. M. Collins, "Robust simultaneous detection of coronary borders in complex images," *IEEE Trans. Med. Imag.*, vol. 14, no. 1, pp. 151–161, Mar. 1995.

[171] J. H. C. Reiber, C. J. Kooijman, C. J. Slager, J. J. Gerbrands, J. C. H. Schuurbiers, A. D. Boer, W. Wijns, P. W. Serruys, and P. G. Hugenholtz, "Coronary artery dimensions from cineangiograms - methodology and validation of a computer-assisted analysis procedure," *IEEE Trans. Med. Imag.*, vol. 3, no. 3, pp. 131–141, Sep. 1984.

[172] Y. Sun, "Automated identification of vessel contours in coronary arteriograms by an adaptive tracking algorithm," *IEEE Trans. Med. Imag.*, vol. 8, no. 1, pp. 78–88, Mar. 1989.

[173] A. K. Klein, F. Lee, and A. A. Amini, "Quantitative coronary angiography with deformable spline models," *IEEE Trans. Med. Imag.*, vol. 16, no. 5, pp. 468–482, Oct. 1997.

[174] Y. Zhou, A. Kaufman, and A. W. Toga, "Three-dimensional skeleton and centerline generation based on an approximate minimum distance field," *Visual Comput.*, vol. 14, no. 7, pp. 303–314, 1998.

[175] Y. Zhou and A. W. Toga, "Efficient skeletonization of volumetric objects," *IEEE Trans. Visual. Comput. Graphics*, vol. 5, no. 3, pp. 196–209, 1999.

[176] X. Xie and M. Mirmehdi, "Magnetostatic field for the active contour model: A study in convergence," in *Proc. British Mach. Vis. Conf.*, 2006, pp. 127–136.

[177] S. Y. Yeo, X. Xie, I. Sazonov, and P. Nithiarasu, "Geometric potential force for the deformable model," in *Proc. British Mach. Vis. Conf.*, 2009, pp. 1–11.

[178] E. Sifakis, C. Garcia, and G. Tziritas, "Bayesian level sets for image segmentation," *J. Vis. Commun. Image Rep.*, vol. 13, pp. 44–64, 2002.

[179] J. Nocedal and S. Wright, *Numerical Optimization.* New York: Springer, 1999.

[180] T. McInerney and D. Terzopoulos, "T-snakes: Topology adaptive snakes," *Med. Imag. Anal.*, vol. 4, no. 2, pp. 73–91, 2000.

[181] A. H. Hernandez, D. G. Gil, P. R. Radeva, and E. N. Nofrerias, "Anisotropic processing of image structures for adventitia detection in intravascular ultrasound images," in *Proc. Computers in Cardiology*, 2004, pp. 229–232.

[182] M. Plissiti, D. I. Fotidadis, L. K. Michalis, and G. E. Bozios, "An automated method for lumen and media-adventitia border detection in a sequence of ivus frames," *IEEE Trans. Info. Tech. Biomed.*, vol. 8, no. 2, pp. 131–141, Jun. 2004.

[183] X. Xie and M. Mirmehdi, "Level-set based geometric colour snake with region support," in *Proc. IEEE Int. Conf. Image Processing*, 2003, pp. 153–156.

[184] J.-L. Jones, E. Essa, X. Xie, and D. Smith, "Interactive segmentation of media-adventitia border in IVUS," in *Proc. Int. Conf. Computer Analysis of Images and Patterns*, 2013, pp. 466–474.

[185] J.-L. Jones, X. Xie, and E. Essa, "Combining region-based and imprecise boundary-based cues for interactive medical image segmentation," *Int. J. Numerical Methods in Biomed. Eng.*, vol. 30, no. 12, pp. 1649–1666, Dec. 2014.

[186] X. Xie and M. Mirmehdi, "Implicit active model using radial basis function interpolated level sets," in *Proc. British Mach. Vis. Conf.*, 2007, pp. 1040–1049.

[187] S. Y. Yeo, X. Xie, I. Sazonov, and P. Nithiarasu, "Level set segmentation with robust image gradient energy and statistical shape prior," in *Proc. IEEE Int. Conf. Image Processing*, 2011, pp. 3397–3400.

[188] Y. Boykov and G. Funka-Lea, "Graph cuts and efficient N-D image segmentation," *Int. J. Comput. Vis.*, vol. 70, no. 2, pp. 109–131, 2006.

[189] A. Paiement, M. Mirmehdi, X. Xie, and M. Hamilton, "Integrated segmentation and interpolation of sparse data," *IEEE Trans. Imag. Proc.*, vol. 23, no. 1, pp. 110–125, Jan. 2014.

[190] A. F. Frangi, W. J. Niessen, and M. A. Viergever, "Three-dimensional modeling for functional analysis of cardiac images: a review," *IEEE Trans. Med. Imag.*, vol. 20, no. 1, pp. 2–25, Jan. 2001.

[191] J. Weng, A. Singh, and M. Y. Chiu, "Learning-based ventricle detection from cardiac MR and CT images," *IEEE Trans. Med. Imag.*, vol. 16, no. 4, pp. 378–391, Aug. 1997.

[192] T. F. Cootes, G. J. Edwards, and C. J. Taylor, "Active appearance models," in *Proc. European Conf. Comput. Vis.*, 1998, pp. 484–498.

[193] M.-P. Jolly, N. Duta, and G. Funka-Lea, "Segmentation of the left ventricle in cardiac MR images," in *Proc. IEEE Int. Conf. Comput. Vis.*, 2001, pp. 501–508.

[194] T. Saito, M. Misaki, K. Shirato, and T. Takishima, "Three-dimensional quantitative coronary angiography," *IEEE Trans. Biomed. Eng.*, vol. 37, no. 8, pp. 768–777, Aug. 1990.

[195] S. R. Fleagle, M. R. Johnson, C. J. Wilbricht, D. J. Skorton, R. F. Wilson, C. W. White, M. L. Marcus, and S. M. Collins, "Automated analysis of coronary arterial morphology in cineangiograms: Geometric and physiologic validation in humans," *IEEE Trans. Med. Imag.*, vol. 8, no. 4, pp. 387–400, Dec. 1989.

[196] I. Liu and Y. Sun, "Recursive tracking of vascular networks in angiograms based on detection-deletion scheme," *IEEE Trans. Med. Imag.*, vol. 12, no. 2, pp. 334–341, Jun. 1993.

[197] K. Haris, S. N. Efstratiadis, N. Maglaveras, C. Pappas, J. Gourassas, and G. Louridas, "Model-based morphological segmentation and labeling of coronary angiograms," *IEEE Trans. Med. Imag.*, vol. 18, no. 10, pp. 1003–1015, Oct. 1999.

[198] C. Blondel, G. Malandain, R. Vaillant, and N. Ayache, "Reconstruction of coronary arteries from a single rotational X-ray projection sequence," *IEEE Trans. Med. Imag.*, vol. 25, no. 5, pp. 653–663, May 2006.

[199] J. A. Tyrrell, E. di Tomaso, D. Fuja, R. Tong, K. Kozak, R. K. Jain, and B. Roysam, "Robust 3-D modeling of vasculature imagery using superellipsoids," *IEEE Trans. Med. Imag.*, vol. 26, no. 2, pp. 223–237, Feb. 2007.

[200] A. Narayanaswamy, S. Dwarakapuram, C. S. Bjornsson, B. M. Cutler, W. Shain, and B. Roysam, "Robust adaptive 3-D segmentation of vessel laminae from fluorescence confocal microscope images and parallel GPU implementation," *IEEE Trans. Med. Imag.*, vol. 29, no. 3, pp. 583–597, Mar. 2010.

[201] W. C. K. Wong, R. W. K. So, and A. C. S. Chung, "Principal curves for lumen center extraction and flow channel width estimation in 3-D arterial networks: Theory, algorithm, and validation," *IEEE Trans. Imag. Proc.*, vol. 21, no. 4, pp. 1847–1862, Apr. 2012.

[202] Y. Wang and P. Liatsis, "3-D quantitative vascular shape analysis for arterial bifurcations via dynamic tube fitting," *IEEE Trans. Biomed. Eng.*, vol. 59, no. 7, pp. 1850–1860, Jul. 2012.

[203] A. Hernandez-Vela, C. Gatta, S. Escalera, L. Igual, V. Martin-Yuste, M. Sabate, and P. Radeva, "Accurate coronary centerline extraction, caliber estimation, and catheter detection in angiographies," *IEEE Trans. Info. Tech. Biomed.*, vol. 16, no. 6, pp. 1332–1340, Nov. 2012.

[204] S. Cetin, A. Demir, A. Yezzi, M. Degertekin, and G. Unal, "Vessel tractography using an intensity based tensor model with branch detection," *IEEE Trans. Med. Imag.*, vol. 32, no. 2, pp. 348–363, Feb. 2013.

[205] M.-P. Garcia, J. Velut, D. Boulmier, C. Leclercq, M. Garreau, P. Haigron, and C. Toumoulin, "Coronary vein extraction in MSCT volumes using minimum cost path and geometrical moments," *IEEE J. Biomed. Health Infor.*, vol. 17, no. 2, pp. 336–345, Mar. 2013.

[206] Y. Wang, C. Toumoulin, H. Z. Shu, Z. D. Zhou, and J. L. Coatrieux, "Vessel extraction in coronary X-ray angiography," in *Proc. IEEE Int. Conf. Eng. Med. Bio. Soc.*, 2005, pp. 1584–1587.

[207] R. Manzke, V. Y. Reddy, S. Dalal, A. Hanekamp, V. Rasche, and R. C. Chan, "Intra-operative volume imaging of the left atrium and pulmonary veins with rotational X-ray angiography," in *Proc. Med. Image Comput. Comput. Assist. Interv.*, 2006, pp. 604–611.

[208] A. Thiagalingam, R. Manzke, A. D'Avila, I. Ho, A. Locke, J. Ruskin, R. Chan, and V. Reddy, "Intraprocedural volume imaging of the left atrium and pulmonary veins with rotational X-ray angiography: Implications for catheter ablation of atrial fibrillation," *J. Cardiovasc. Electrophysiol.*, vol. 19, no. 3, pp. 293–300, Mar. 2008.

[209] J. Ector, S. D. Buck, J. Adams, S. Dymarkowski, J. Bogaert, F. Maes, and H. Heidbuchel, "Cardiac three-dimensional magnetic resonance imaging and fluoroscopy merging: A new approach for electroanatomic mapping to assist catheter ablation," *Circulation*, vol. 112, no. 24, pp. 3769–3776, Dec. 2005.

[210] J. Dong, H. Calkins, S. B. Solomon, S. Lai, D. Dalal, A. C. Lardo, E. Brem, A. Preiss, R. D. Berger, H. Halperin, and T. Dickfeld, "Integrated electroanatomic mapping with three-dimensional computed tomographic images for real-time guided ablations," *Circulation*, vol. 113, no. 2, pp. 186–194, Jan. 2006.

[211] Z. Malchano, P. Neuzil, R. Cury, G. Holmvang, J. Weichet, E. Schmidt, J. Ruskin, and V. Reddy, "Integration of cardiac CT/MR imaging with three-dimensional electroanatomical mapping to guide catheter manipulation in the left atrium: Implications for catheter ablation of atrial fibrillation," *J. Cardiovasc. Electrophysiol.*, vol. 17, no. 11, pp. 1221–1229, Nov. 2006.

[212] V. Y. Reddy, Z. J. Malchano, G. Holmvang, E. J. Schmidt, A. d'Avila, C. Houghtaling, R. C. Chan, and J. N. Ruskin, "Integration of cardiac magnetic resonance imaging with three-dimensional electroanatomic mapping to guide left ventricular catheter manipulation," *J. Am. Coll. Cardiol.*, vol. 44, no. 11, pp. 2202–2213, Dec. 2004.

[213] M. Sonka, M. D. Winniford, X. Zhang, and S. M. Collins, "Lumen centerline detection in complex coronary angiograms," *IEEE Trans. Biomed. Eng.*, vol. 41, no. 6, pp. 520–528, Jun. 1994.

[214] H. Greenspan, M. Laifenfeld, S. Einav, and O. Barnea, "Evaluation of center-line extraction algorithms in quantitative coronary angiography," *IEEE Trans. Med. Imag.*, vol. 20, no. 9, pp. 928–941, Sep. 2001.

[215] M. Schaap, et al., "Standardized evaluation methodology and reference database for evaluating coronary artery centerline extraction algorithms," *Med. Imag. Anal.*, vol. 13, no. 5, pp. 701–714, 2009.

[216] P. Jannin, J. M. Fitzpatrick, D. J. Hawkes, X. Pennec, R. Shahidl, and M. W. Vannier, "Validation of medical image processing in image-guided therapy," *IEEE Trans. Med. Imag.*, vol. 21, no. 12, pp. 1445–1449, 2002.

[217] J. K. Udupa, V. R. LeBlanc, Y. Zhuge, C. Imielinska, H. Schmidt, L. M. Currie, B. E. Hirsch, and J. Woodburn, "A framework for evaluating image segmentation algorithms," *Comput. Med. Imag. Graphics*, vol. 30, no. 2, pp. 75–87, Mar. 2006.

[218] A. Popovic, M. de la Fuente, M. Engelhardt, and K. Radermacher, "Statistical validation metric for accuracy assessment in medical image segmentation," *Int. J. Comput. Assisted Radiol. Surg.*, vol. 2, no. 3-4, pp. 169–181, Dec. 2007.

[219] M. Prastawa, E. Bullitt, S. Ho, and G. Gerig, "Robust estimation for brain tumor segmentation," in *Proc. Med. Image Comput. Comput. Assist. Interv.*, 2003, pp. 530–537.

[220] Z. Y. Shan, Q. Ji, A. Gajjar, and W. E. Reddick, "A knowledge-guided active contour method of segmentation of cerebella on MR images of pediatric patients with medulloblastoma," *J. Magn. Reson. Imag.*, vol. 21, no. 1, pp. 1–11, Jan. 2005.

[221] K. H. Zou, S. K. Warfield, A. Bharatha, C. M. C. Tempany, M. R. Kaus, S. J. Haker, W. M. Wells III, F. A. Jolesz, and R. Kikinis, "Statistical validation of image segmentation quality based on a spatial overlap index," *Acad. Radiol.*, vol. 11, no. 2, pp. 178–189, Feb. 2004.

[222] K. H. Zou, W. M. Wells III, R. Kikinis, and S. K. Warfield, "Three validation metrics for automated probabilistic image segmentation of brain tumours," *Statist. Med.*, vol. 23, no. 8, pp. 1259–1282, Apr. 2004.

[223] Y. Yitzhaky and E. Peli, "A method for objective edge detection evaluation and detector parameter selection," *IEEE Trans. Pattern Anal. Mach. Intell.*, vol. 25, no. 8, pp. 1027–1033, Aug. 2003.

[224] T. A. Lasko, J. G. Bhagwat, K. H. Zou, and L. Ohno-Machado, "The use of receiver operating characteristic curves in biomedical informatics," *J. Biomed. Infor.*, vol. 38, no. 5, pp. 404–415, Oct. 2005.

[225] A. P. Zijdenbos, B. M. Dawant, R. A. Margolin, and A. C. Palmer, "Morphometric analysis of white matter lesions in mr images: method and validation," *IEEE Trans. Med. Imag.*, vol. 13, no. 4, pp. 716–724, Dec. 1994.

Feng Zhao received the B.Eng. degree in electronic engineering from the University of Science and Technology of China, Hefei, China, in 2000 and the M.Phil. and Ph.D. degrees in computer vision from The Chinese University of Hong Kong, Hong Kong, in 2002 and 2006, respectively. From June 2006 to September 2007, he was a Postdoctoral Fellow in the Department of Information Engineering, The Chinese University of Hong Kong. From October 2007 to July 2010, he was a Research Fellow at the School of Computer Engineering, Nanyang Technological University, Singapore. After that, he worked as a Postdoctoral Research Associate in the Intelligent Systems Research Centre, University of Ulster, U.K. Since November 2011, he has been with the Department of Computer Science, Swansea University, Swansea, U.K., where he is currently a Workshop Developer and a Postdoctoral Fellow. His research interests include image processing, biomedical image analysis, computer vision, pattern recognition, and machine learning.
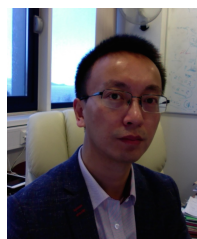
Xianghua Xie is an Associate Professor in the Visual Computing Group at the Department of Computer Science, Swansea University. He held an RCUK Academic Fellowship between September 2009 and March 2012, and he was a Senior Lecturer between October 2012 and March 2013. Prior to his position at Swansea, he was a Research Associate in the Computer Vision Group, Department of Computer Science, University of Bristol, where he obtained his PhD in Computer Science and MSc in Advanced Computing (with commendation) in 2006 and 2002, respectively. He has strong research interests in video analysis, stereo systems, active contour models, level set methods, texture analysis, and medical image understanding. He leads a team of researchers at Swansea University in these areas, and has published just under 100 papers in computer vision and pattern recognition. He is associate editor of IET Computer Vision, and general chair of BMVC2015 and MIUA2012. He is a senior member of IEEE and an executive committee member of BMVA.

Matthew Roach received a BEng (Hons) degree in Electronic Engineering from Swansea University in 1998, and in 2002 he graduated with a PhD funded by the EPSRC and BT (British Telecom). Matt held a Senior Research Assistant position in the Speech and Image Processing Group in Swansea until 2002, working on classification of video signals for next generation TV funded by BT. From 2002 to 2004, Matt worked for a systems engineering company working with a number of blue chip organisations. During 2004-2010, he ran a software development firm specialising in web-based software development for service-based businesses. Matt has been working in the Computer Science Department at Swansea University since 2010, building applied research partnerships. His current research interests include machine learning, pattern recognition, and data mining. Matt is a member of the IET.